Linking Gulf Stream Air-Sea Interactions to the Exceptional Blocking Episode in February 2019: A Lagrangian Perspective

Marta Wenta[1], Christian M. Grams[1], Lukas Papritz[2], and Marc Federer[2]

[1]Institute of Meteorology and Climate Research, Department Troposphere Research (IMK-TRO), Karlsruhe Institute of Technology (KIT), Karlsruhe, Germany

[2]Institute for Atmospheric and Climate Science, ETH Zürich, Zurich, Switzerland

Correspondence: Marta Wenta (marta.wenta@kit.edu)

Abstract.

The development of atmospheric blocks over the North Atlantic European region can lead to extreme weather events like heatwaves or cold air outbreaks. Despite their potential severe impact on surface weather, the correct prediction of blocking lifecycles remains a key challenge in current numerical weather prediction (NWP) models. Increasing evidence suggests that latent heat release in cyclones, the advection of cold air (cold air outbreaks, CAOs) from the Arctic over the North Atlantic, and associated air-sea interactions over the Gulf Stream are key processes responsible for the onset, maintenance, and persistence of such flow regimes. To better understand the mechanism connecting air-sea interactions over the Gulf Stream with changes in the large-scale flow, we focus on an episode between 20 and 27 of February 2019, when a quasi-stationary upper-level ridge was established over western Europe accompanied by an intensified storm track in the Northwestern North Atlantic. During that time, a record-breaking winter warm spell occurred over Western Europe bringing temperatures above 20°C to the United Kingdom, the Netherlands, and Northern France. The event was preceded and accompanied by the development of several rapidly intensifying cyclones that originated in the Gulf Stream region and traversed the North Atlantic. To explore the mechanistic linkage between the formation of this block and air-sea interactions over the Gulf Stream, we adopt a Lagrangian perspective, using kinematic trajectories. This allows us to study the pathways and transformations of air masses that form the upper-level potential vorticity anomaly and interact with the ocean front. We establish that more than one-fifth of these air masses interact with the Gulf Stream in the lower troposphere, experiencing intense heating and moistening over the region, due to the frequent occurrence of CAOs behind the cold front of the cyclones. Trajectories moistened by the advection of cold air over warm ocean by one cyclone, later ascend into the upper troposphere with the ascending air stream of a consecutive cyclone, fueled by the strong surface fluxes. These findings highlight the importance of CAOs in the Gulf Stream region with their intense coupling between the ocean and atmosphere for blocking development and provide a mechanistic pathway linking air-sea interactions in the lower troposphere and the upper-level flow.

1 Introduction

Atmospheric blocks are quasi-stationary anticyclonic circulation anomalies disrupting the eastward propagation of synoptic weather systems. The associated high-pressure system can dominate the weather over a particular location for an extended

period of time, from several days to weeks (Wazneh et al., 2021) and lead to the development of extreme weather, like cold spells (e.g. de'Donato et al., 2013; Demirtaş, 2017; Pang et al., 2020; Zhuo et al., 2022) and heatwaves (e.g. Grumm, 2011; Barriopedro et al., 2011; Spensberger et al., 2020; Dae et al., 2022; Kautz et al., 2022) with significant socio-economic impacts. Despite ongoing development and increasing resolution of numerical climate and weather prediction models, the correct prediction of those quasi-stationary weather patterns still poses a challenge (Matsueda and Palmer, 2018; Ferranti et al., 2018; Grams et al., 2018; Büeler et al., 2021).

The dynamics of cyclones and blocking anticyclones are mutually linked with the position and tilt of the upper-tropospheric jet. The crucial role of cyclones for the formation and maintenance of the blocks has been established by multiple studies (e.g. Colucci, 1985; Colucci and Alberta, 1996; Lupo and Smith, 1995; Nakamura and Wallace, 1993; Mullen, 1987; Yamazaki and Itoh, 2009). The development of cyclones results in the cross-isentropic ascent of air from the lower to the upper troposphere, in the so-called Warm Conveyor Belt (WCB; Wernli and Davies, 1997; Madonna et al., 2014; Pfahl et al., 2014). Condensation and resulting latent heat release during the ascent are critical for both cyclone intensification, through the production of potential vorticity (PV) below the level of maximum heating (Binder et al., 2016; Reed et al., 1992; Čampa and Wernli, 2012), and growth of the upper-level ridge, due to the destruction of PV above the level of maximum heating (Methven, 2015; Madonna et al., 2014; Joos and R.M.Forbes, 2016; Grams et al., 2011). The injection of low PV air into the upper troposphere together with diabatically enhanced divergent outflow amplifies and reinforces the upper-tropospheric ridge (Grams et al., 2011; Teubler and Riemer, 2016; Grams and Archambault, 2016; Steinfeld and Pfahl, 2019). Diabatic processes, as recently quantified by Pfahl et al. (2015); Steinfeld and Pfahl (2019); Steinfeld et al. (2020); Yamamoto et al. (2021) are in many cases essential for the development of blocks in the North Atlantic-European region. In fact, recent studies indicate that the duration, strength, and possibly even formation of the block are influenced by latent heat release in the ascending air streams (Steinfeld et al., 2020; Pfahl et al., 2015).

The key role of moist dynamics in blocking formation and development suggests that there exists a relationship between upstream, lower-tropospheric processes and the formation of the upper-level, quasi-stationary ridge. The air masses that undergo latent heat release during the ascent in the warm sector of the cyclone need to first pass through a region of intense surface evaporation to pick up a sufficient amount of moisture. Recent studies suggest that during winter the moisture source locations of cyclone precipitation are fairly local and over the ocean (Pfahl et al., 2014; Papritz et al., 2021). In the North Atlantic, the most intense evaporation events are associated with the Gulf Stream (Aemisegger and Papritz, 2018). The propagation of cyclones across the Gulf Stream region provides conditions for large surface latent and sensible heat fluxes (Tilinina et al., 2018; Moore and Renfrew, 2002), due to the development of CAOs and the descent of dry air in the cold sector (Vannière et al., 2017b; Raveh-Rubin, 2017; Aemisegger and Papritz, 2018). The warm waters of the Gulf Stream have been identified by Papritz et al. (2021) as a primary moisture source for cyclone-related precipitation in the North Atlantic. Papritz et al. (2021) demonstrated also that air masses moistened and heated in the cold sector of one cyclone are then brought into the warm sector of the consecutive cyclone through a cyclone relative flow, called feeder air stream (Dacre et al., 2019). This type of cyclone-cyclone interaction has been previously identified by Sodemann and Stohl (2013) and termed a 'hand-over' mechanism. Furthermore, Boutle et al. (2011) supports this understanding, having established that the moisture adjustment timescale in the boundary

layer is approximately 2.3 days. Moreover, intense turbulent heat fluxes during CAO events also play a crucial role in the restoration of baroclinicity in the lower troposphere (Papritz and Spengler, 2015; Vannière et al., 2017b), and precondition the atmosphere for the development of consecutive low-pressure systems (Tilinina et al., 2018; Papritz et al., 2021; Vannière et al., 2017a). In consequence, CAOs can regulate cyclone formation and strength and hence potentially affect downstream large-scale dynamics (Papritz and Grams, 2018).

Previous studies demonstrated that intense heat transfer in the regions of western boundary currents influences the position of the storm tracks (Kwon et al., 2010; Shaw et al., 2016) and plays an important role in the upper-level jet variability (Nakamura et al., 2008). In fact, Kwon et al. (2010) found in their modeling study that the absence of the Gulf Stream sea surface temperature (SST) gradient results in a reduced frequency of blocks downstream. Furthermore, O'Reilly et al. (2017) determined that wintertime poleward displacements of the jet stream are preceded by high eddy heat fluxes over the Gulf Stream and western North Atlantic. The mechanism behind those displacements is explained by Novak et al. (2015) and Kwon et al. (2020), who showed that the shift of the upper-level flow is caused by the northward shift of eddy heat flux in the lower troposphere. An increasing number of studies also indicate that the Gulf Stream region might serve as a moisture source for air masses ascending into the blocking regions. Yamamoto et al. (2021), using a 31-year climatology of backward air trajectories started from the upper-level North Atlantic-European blocks, found that the Atlantic basin provides most of the moisture for the moist air masses ascending into the block. Moreover, they established that trajectories that gather moisture from the ocean follow the path of the Gulf Stream and identified the region of the SST gradient in the western North Atlantic as the region where trajectories ascent to the upper troposphere. Those results are also in agreement with the findings of Pfahl et al. (2014), who determined that moisture supplies for WCBs are collocated with the regions of intense ocean evaporation in the western North Atlantic.

Throughout the literature, researchers have established the importance of ocean-atmosphere coupling over the Gulf Stream and its relevance for downstream large-scale dynamics (e.g. Vannière et al., 2017b; Sheldon et al., 2017; Papritz and Spengler, 2015). However, the scientific community has yet to gain a clear understanding of the physical pathway through which signals from individual processes in the marine boundary layer are conveyed to the large-scale circulation (Czaja et al., 2019). In this study, we propose a possible explanation for this missing mechanistic link by conducting a case study of European Blocking from February 2019. This event brought record-breaking winter "heat" to Western Europe and was accompanied by a series of upstream, rapidly intensifying cyclones. We investigate the potential connections between air-sea interactions over the Gulf Stream region and the formation of an upper-level ridge over western Europe using a Lagrangian perspective in a synoptic analysis. The paper is structured as follows: First, we provide a detailed description of the data and methods, including trajectory calculations (Section 2). Second, we introduce the European Blocking case study of February 2019 (Section 3.1). In the subsequent section, we provide a detailed description of our analysis results, examining the characteristics of air masses that interact with the Gulf Stream and assessing their links to cold air outbreaks and cyclones (Section 3.2). Then, we analyze the moisture sources and transport paths of the air ascending into the block (Section 3.3). Finally, we discuss our findings and establish a connection between air-sea interactions over the Gulf Stream, cyclone development, and the potential influence of these air masses on atmospheric blocking events.

2 Methodology

2.1 Data

2.1.1 ERA5 reanalysis

The calculation of kinematic trajectories and the analyses presented in this study are based on the European Center for Medium-Range Weather Forecasts (ECMWF) reanalysis - ERA5 (Hersbach et al., 2020). For most of the study, we use reanalysis data at the 3-hourly temporal resolution, interpolated on a 0.5°x0.5° horizontal grid. In addition, we employ ERA5 data with a higher temporal resolution of one hour for the investigation of cyclone tracks (Section 3), the vertical and horizontal distribution of negative potential vorticity, potential temperature, and the cloud liquid water content (Appendix A). We chose the lower 98 sigma-pressure vertical levels out of a total of 137 available levels for our investigation, covering the pressure range from $\sim$26 hPa to the surface. The analyzed data covers the period from 10 to 28 February 2019.

2.1.2 Cyclone dataset

The cyclone tracks are obtained using the method of Sprenger (2017) and Wernli and Schwierz (2006), based on the identification and tracking of the sea level pressure (SLP) minima, defined as the grid points with SLP value lower than at all the neighboring grid points (eight in our case). In addition, the cyclone extent is determined by the outermost closed SLP contour surrounding the identified SLP minimum. This is limited to areas beyond 25° N/S, with a contour circumference cap at 7500 km. This approach ensures the exclusion of SLP minima linked to tropical convection and overly extensive cyclone masks that encompass multiple cyclones. The tracking algorithm is applied to hourly fields of SLP from ERA5 reanalysis. Rapidly intensifying cyclones are identified using the criterion of Sanders and Gyakum (1980) of a central pressure drop of at least 24 hPa within 24 hours. This criterion is further normalized using the factor $\sin(60°)/\sin\phi$, where ϕ represents the average latitude of the cyclone's center during the given time span.

2.1.3 Identification of the block and upper-troposphere negative potential vorticity anomalies.

The European Block in February 2019 is identified using the year-round weather regime definition of Grams et al. (2017) for the North Atlantic-European region. The block is characterized by a positive geopotential height anomaly over the eastern North Atlantic and Europe and a negative geopotential height anomaly upstream over Greenland. The methodology for identifying specific weather regimes is described in detail in Grams et al. (2017) and Hauser et al. (2022).

The formation of the atmospheric block in the Euro-Atlantic region is associated with the poleward advection of low PV air. The accumulation of low PV air in the upper troposphere leads to the development of negative potential vorticity anomalies (NPVA; Teubler and Riemer, 2016), which amplify the upper-level ridge. In our study, we use the method of Hauser et al. (2022) to identify NPVAs in the ERA5 dataset. First, the deviations of PV from a 30-day running mean climatology (1979-2019) centered on the day of interest are calculated. Then, vertical averages of obtained values between 500 and 150 hPa are computed and labeled as NPVA objects if they fall below the threshold of -0.8 PVU. In the next step, a quasi-Lagrangian

framework is employed to follow the evolution of NPVAs and assign them to the lifecycle of the European Block in February 2019. PVAs are assigned to an active weather regime (European Block) based on their spatial overlap with a predefined regime mask. The mask is defined as the area where the vertical average PV anomaly of the composite for the respective weather regime is below -0.3 PVU. The composite is determined by averaging the PV between 500 and 150 hPa during the active phase of a weather regime (in our case European Block, as defined by Grams et al. (2017)). If there is at least a 10% overlap between a PVA and this mask during an active phase, we associate it with that specific regime's life cycle. Note that a single regime can sometimes be influenced by several PVAs.

The formation of the studied block was related to one major NPVA which formed 10 days prior to blocking onset, and another minor NPVA that appeared on 23 February over Greenland (Fig.2). The major NPVA originated in the North Pacific and started to strengthen a few days before the block onset when it propagated into the North Atlantic. For the purpose of the present study, we neglect the NPVAs lifecycle prior to their arrival into the North Atlantic region.

2.1.4 Identification of cold air outbreaks

Cold air outbreaks (CAO) in the ERA5 dataset are identified using the method of Papritz et al. (2015). First, the air-sea potential temperature difference between $\theta_{SST} - \theta_{850}$ is calculated, where θ_{SST} denotes sea surface potential temperature and θ_{850} air potential temperature at 850 hPa. The reference pressure p_0 =1000 hPa is used for the calculation of surface potential temperature. In agreement with Papritz et al. (2015), we require the $\theta_{SST} - \theta_{850}$ over the ocean to exceed 0 K to identify the CAO events.

To determine if a trajectory (Section 2.2) is a part of a CAO, we consider $\theta_{SST} - \theta$, where θ is the air parcel potential temperature (see Papritz and Spengler (2017)). If the potential temperature of an air parcel (at a pressure greater than 850 hPa) is lower than the SST beneath it, we classify the trajectory as a CAO trajectory.

2.2 Trajectory datasets

The LAGRANTO analysis tool (LAGRANTO Sprenger and Wernli, 2015) is employed to calculate kinematic trajectories, using three-dimensional wind on model levels from the ERA5 dataset described above. Output positions of trajectories are available in 3-hourly intervals and the following variables are traced along the trajectories: pressure height (p), temperature (T), specific humidity (Q), potential vorticity (PV), potential temperature (θ), surface pressure (PS), surface latent heat flux ($SLHF$), surface sensible heat flux ($SSHF$), boundary layer height (BLH) and sea surface temperature (SST). We have created a primary trajectory dataset, termed NPVA base trajectories (Tab.1). This dataset is further filtered in order to work out the relationship between the atmospheric block and air-sea interactions over the Gulf Stream (GS), and to examine the specific properties of the trajectories (Appendix A). The main trajectory subsets, which are crucial to this manuscript, are outlined in Tab.1, relative fractions shown in Tab.2, and will be discussed in subsequent sections.

Name of the dataset	Starting area	Duration of the trajectories	Characteristics
NPVA base trajectories	Upper troposphere NPVA.	-10 days	Started from the NPVA objects related to the European Blocking event in February 2019.
Subsets (NPVA base trajectories)			
NPVA no ascent trajectories	Upper troposphere NPVA.	-10 days	Trajectories that do not fulfill the ascent criterium of 500 hPa within 10 days backward.
NPVA trajectories			**Ascent of 500 hPa within 10 days prior to the arrival in NPVA.**
Subsets (NPVA trajectories)			
NPVA GS trajectories	**Upper troposphere NPVA.**	**-10 days**	**Interact with the ABL over the Gulf Stream.**
NPVA nonGS trajectories			**Do not interact with the ABL over the Gulf Stream.**

Table 1. Overview of the trajectory subsets used in the study. The data sets primarily used in the study are highlighted in bold font.

2.2.1 NPVA Trajectories

The base trajectory dataset comprises 10-day backward trajectories started from the upper-level NPVA objects (Section 2.1.3) every 3 hours between 20 February 09:00 UTC and 28 February 12:00 UTC (NPVA base trajectories, Tab.1). Those 10-day kinematic backward trajectories are initiated from equidistant grid points of size 100x100 km. Vertically, the starting points span from 500 to 150 hPa within both NPVAs, with an interval of Δp=25 hPa. To avoid the possibility of trajectory double-counting, we remove those that remain for two consecutive time steps within the starting grid of the NPVA. This filtering technique removes approximately 10% of trajectories, ensuring that we do not count the same air mass multiple times.

In the consecutive analysis, the obtained trajectory dataset is refined as we apply additional selection criteria. To select only the ascending trajectories, we require trajectories to experience a pressure decrease of 500 hPa within 10 days prior to the arrival in the upper-level NPVA, hence the air parcel can ascend at any time and any rate (NPVA trajectories, Tab.1). The threshold of 500 hPa is chosen to ensure that the trajectory has ascended all the way from the lower troposphere and is motivated by common criteria to identify WCB air streams (e.g. Madonna et al., 2014). However, it is a bit weaker and allows ascending motion over a longer time span enabling the analysis of ocean influence on the ascending air also independent of WCB activity. Approximately 43% of the NPVA base trajectories experience such an ascent of 500 hPa before their arrival into the upper-level NPVA. Those ascending and filtered trajectories will be referred to throughout the following analysis as 'NPVA trajectories' (Tab.1).

For the ascending NPVA trajectories and their subsets (NPVA GS and NPVA nonGS) we further refer to their inflow, ascent, and outflow stages. Therefore at a given time, we identify the position of air parcels from all trajectories with different trajectory starting times and group them in an inflow ($p >$800 hPa), ascent (800$\leq p \leq$400 hPa), and outflow ($p <$400 hPa)layer. The boundaries of layers are motivated by similar layers used for classifying WCB air streams (e.g. Binder et al., 2020).

2.2.2 NPVA GS Trajectories

Taking into account the importance of the Gulf Stream for the selected study, we create an additional subset of trajectories consisting of only those NPVA trajectories that have passed over the Gulf Stream in the lower troposphere. We define the boundary for the lower troposphere at 800 hPa, which is commonly used as an upper boundary of the layer in which the ascending WCB air stream has its inflow and gains moisture (e.g. Binder et al., 2020). The region of the Gulf Stream (GS

masks) is defined for every 3-hourly timestep of the ERA5 dataset for February 2019 using the following steps: (i) first, the horizontal gradient of the SST is identified in both west-east and north-south directions, (ii) a threshold of $|\nabla SST| > 2\,\mathrm{K}$ is applied to extract the area of the Gulf Stream SST front, (iii) a buffer of 100 km is added to the identified gradient, creating a continuous region.

In the following, we refer to those trajectories as 'NPVA GS trajectories' (Tab.1). The rest of the trajectories, i.e. those that did not interact with the ABL over the Gulf Stream, are labeled as 'NPVA nonGS trajectories' (Tab.1).

For each trajectory within the NPVA GS and NPVA nonGS datasets, we pinpoint the onset of ascent. This specific moment is identified when the trajectory's pressure first drops below 800 hPa. After this, the trajectory consistently rises until it reaches the upper troposphere, marked by pressures falling below 500 hPa.

2.3 Moisture source identification

The method of Sodemann et al. (2008) is applied for the purpose of moisture source identification. In this approach, a specific humidity change along a trajectory is considered as an uptake if the specific humidity difference between two-time steps (difference of 3 h) exceeds 0.02 g/kg. Each uptake is given a weight based on all consecutive changes in the specific humidity along the trajectory. This means that the contribution of each uptake is adjusted by considering precipitation events en route and subsequent uptakes. This method has been widely recognized as appropriate for the identification of moisture sources and used in a number of other studies (e.g. Papritz et al., 2021; Xin et al., 2022; Jullien et al., 2020; Aemisegger and Papritz, 2018).

This method is applied to both the NPVA GS and the NPVA nonGS trajectories to identify the sources of moisture present at the start of the ascent. The use of the start of the trajectory's ascent as a reference time for the moisture diagnostic allows us to identify the sources of moisture contributing to latent heat release during an air parcel's upward movement. For the purpose of this analysis, every backward NPVA trajectory (NPVA GS and NPVA nonGS, Tab.1) is extended another 10 days backward from the time when the ascent started.

3 Results

3.1 The European Blocking Heatwave 2019

The European Blocking event in February 2019 lasted for about 7 days, from 20 to 27 February. The duration of this event was below the average for winter block events in the Northern Hemisphere (Wazneh et al., 2021). However, it was accompanied by record high temperatures for this month in France, the Netherlands, and the United Kingdom (Young and Galvin, 2020) with 2 m temperature anomalies in western Europe exceeding +10 °C (Fig.1). This exceptional, wintertime heatwave was linked to the formation of a quasi-stationary upper-level ridge, which brought southerly airflow and clear skies to western Europe (Leach et al., 2021).

Temperature data from weather stations illustrate the extreme nature of this event. The highest temperature anomalies were observed on 26 and 27 February (Fig.1d), with the record high temperature in February for the United Kingdom of 21.2°C

measured in Kew Gardens, London (Young and Galvin, 2020). Record-breaking observations were also made in Scotland (18.3°C), the Netherlands (18.9°C), and Sweden (16.7°C), highlighting the spatial extent of the event (Young and Galvin, 2020).

In the following, we discuss the synoptic evolution based on maps of potential vorticity at 315 K and mean sea level pressure Fig.2. In addition, the tracks of all cyclones during the study period are shown in p Fig. 3. Europe has already experienced moderate winter weather prior to the blocking event. In the second part of February, the upper-level flow was repeatedly interrupted by the formation of upper-tropospheric NPVAs. Two days prior to the analyzed event, on 18 February, the west-to-east propagation of the jet stream was disrupted by the NPVA in the upper troposphere stretching over western Europe and another over the central North Atlantic (white, dashed contours in Fig.2a). Over Europe, this was accompanied by south and southwesterly flow in the western part of the anticyclone bringing high temperatures to western and central Europe with anomalies exceeding 10°C (Fig.1a). On 18 February, the NPVA GS trajectories were found to be in their ascent phase, distinctly spread over the western North Atlantic, as shown by the red crosses in Fig.2a. Yet, the bulk of air parcels that later ascend into the blocking region remained in the lower troposphere. These air parcels were predominantly observed in regions influenced by CAOs in the western and central parts of the North Atlantic (green crosses in Fig.2b). Those CAOs occurred behind the very intensive cyclone L0 (Fig.3a) and ahead of another potent cyclone, L1, emerging near the North American coastline (Fig. 3a). Three days later, the upper-level flow was disturbed by another major NPVA, extending from southern Europe to the North Atlantic and Greenland (magenta shading in Fig.2c). In contrast to the NPVA object from 18 February, this new NPVA became quasi-stationary and persisted over the region for a week. Air parcels in their outflow stage and initially emerging from the Gulf Stream, encompass a notable segment of this major NPVA (black crosses, Fig.2c). In addition, a considerable number of these parcels are in the ascent stage (red crosses, Fig.2c), progressing towards the upper-level ridge. Both the outflow and ascent are potentially linked to the ascending air stream of the rapidly intensifying cyclone L1 (Fig.3a), followed by a smaller cyclogenesis (l1.1, l1.2) in its wake. The transit of this cyclone, characterized by a pressure drop of 39 hPa within 24 h, resulted in the development of a CAO over the western and central North Atlantic, as seen in Fig.2d. This is where the majority of trajectories in the inflow stage (green crosses) are positioned at that moment. On 23 February, the upper-level flow was further disturbed by another minor NPVA (light green in Fig.2e), which strengthened the block and led to its extension westward. This, combined with clear skies and the sustained influx of warm air due to the anticyclonic circulation (Leach et al., 2021), amplified the warm spell across France, the Netherlands, the United Kingdom, and even Scandinavia (Fig.1c). Examining Fig.2e,f, we see distinct patterns. The green crosses in Fig.2f represent trajectories at the inflow stage, while the red and black crosses in Fig.2e correspond to the ascent and outflow stages, respectively. These patterns collectively display a WCB-like structure, directly associated with cyclone L2. This structure not only suggests the genesis of a minor NPVA but also, as indicated by the presence of black crosses in the major NPVA, underscores their potential role in sustaining the block. It is important to highlight the fact that cyclone L2 propagated into the region of high surface fluxes, related to CAOs, left behind by cyclone L1 (Fig.2d). Furthermore, the advection of cold air behind the cold front of L2 resulted in another strong surface evaporation event over the Gulf Stream region (Fig.2f). 27 February marks the last day of the blocking event when the NPVA started to shrink in size and propagate east (Fig.2g) and temperature anomalies in western Europe reached their peak (Fig.1d). Air parcels originating from

	heightWCB (%)	DI(%)	CAO (%)	DI-CAO-DH (%)	DH(%)	$\Delta\theta$K (0-3 days)	Δt of ascent to strongest uptake	Fraction of ascending trajectories (%)	Fraction of all (%)
NPVA GS trajectories	31.2	11.4	82.0	9.11	98	20.77	86	28	12
NPVA nonGS trajectories	29.7	3.71	40.8	2.1	54.7	13.88	67	72	31
NPVA trajectories	29.8	5.99	52	4.24	63.25	16.51	76	100	43
NPVA non ascent trajectories	0	0.67	2.4	0.01	38	8.36	-	0	57
NPVA base trajectories	11.87	2.8	22.3	1.8	48.17	12.66	76	43	100

Table 2. Fractions of various air streams within the NPVA trajectories and the subsets created for the analysis presented in the article. WCB, DI, CAO, DI-CAO-DH, and DH, refer to proporation within their own subset. For NPVA GS, NPVA nonGS, and NPVA trajectories 'Fraction of ascending trajectories' refers to the proportion within NPVA trajectories, which are all ascending. 'Fraction of all' denotes the proportion within the entire set of NPVA base trajectories. $\Delta\theta$K (0-3 days) refers to the change of potential temperature (θ) within 3 days from the start of the trajectories (Pfahl et al., 2015). Δt of ascent to strongest uptake refers to the average time delay between the strongest uptake of trajectories and the time they start ascending later. See Section 3.2 for more details.

trajectories that interacted with the Gulf Stream are predominantly found in the upper troposphere, in the region covered by the NPVA, or in its vicinity (black crosses, Fig.2g). The ascent of those air parcels was most probably associated with cyclones L3 and L4 (Fig.3). Unlike cyclones L1 and L2, the tracks of cyclones L3 and L4 are predominantly constrained to the western North Atlantic. The enhanced outflow from the rising air streams of these cyclones could have played a role in fortifying the upper-level NPVA from a westerly direction, as indicated by the magenta shading and black crosses in Fig.2g. Following the passage of cyclone L3, a subsequent CAO event was observed over the Gulf Stream (Fig.2h). However, unlike earlier events, this CAO was more spatially confined, largely limited to areas near the Gulf Stream.

It should be emphasized that extreme cyclones of 15, 18, 21, and 26 February were accompanied by weaker low-pressure systems developing in the central part of the North Atlantic (light blue lines in Fig.3), bringing the overall count to almost 20 cyclones in the North Atlantic either preceding or concurrent with the blocking event. The evolution of these systems led to the spread of CAOs deeper into the North Atlantic Ocean, resulting in a pervasive presence of intense upward surface fluxes in the region (not shown).

Our synoptic analysis points to a combination of factors that led to the formation of the block in February 2019 and the observed record-high temperatures. The cyclones set the stage for trajectories from the Gulf Stream to move into the upper troposphere. These same cyclones also triggered distinct CAOs in the inflow areas of the trajectories, leading to increased heating and moistening of the atmospheric boundary layer. In the following sections, we will examine the details of NPVA GS trajectories to better understand the evolution of the air masses that interacted with the Gulf Stream.

3.2 Connection between the Gulf Stream region and the large scale dynamics

To investigate a potential link between the Gulf Stream region and the upper-level circulation during the blocking episode, we investigate the characteristics of backward trajectories started in the NPVA objects forming the block in February 2019 (Section 2.2). Given our study's aim to understand how the Gulf Stream influences the upper troposphere, we mainly focus on trajectories that show an ascent of 500 hPa within 10 days backward and that traveled over the Gulf Stream in the lower atmosphere (referred to as NPVA GS trajectories in Tab.1). Out of all the NPVA base trajectories (Tab.1), 43% meet the ascent

criteria, and 28% of those are classified as NPVA GS trajectories (Tab.2). Although NPVA GS trajectories represent just 12% of all trajectories originating from NPVAs (NPVA base trajectories), a focus on these helps to better understand how signals from air-sea interactions over the Gulf Stream propagate to the upper troposphere. Furthermore, as will be shown in the following, their distinct properties hint at a disproportional relevance for the formation and maintenance of the atmospheric block.

First, we examine the differences in pressure changes between NPVA GS and nonGS trajectories. NPVA GS trajectories initially undergo a slight descent from the mid-troposphere towards the atmospheric boundary layer (green shading, Fig.4a). Here, on average, they remain for about 48-72 hours. Then, quite swiftly between -72 h to -36 h, they ascend into the upper troposphere. Conversely, on average NPVA nonGS trajectories start from higher pressure levels, and ascend steadily to the upper troposphere (blue shading, Fig.4a). The ascent of NPVA GS trajectories closely mirrors the distinctive features of the warm conveyor belt (WCB), which typically occurs in the warm sector of extratropical cyclones. As defined by Madonna et al. (2014), a trajectory is denoted as a WCB trajectory if it experiences an ascent of at least 600 hPa within a 48-hour interval. It is crucial to note that their criterion focuses only on the most vigorous part of the air stream that ascends in the warm sector of an extratropical cyclone. Indeed, about 87% of NPVA GS trajectories ascend from pressures greater than 800 hPa to pressures below 500 hPa within only 48 hours, reflecting their relatively fast ascent. Meanwhile, when applying this criterion to NPVA nonGS trajectories, only 72% of them meet the condition.

Applying the strict WCB requirement of 600 hPa ascent within a 48, both NPVA GS and nonGS trajectories comprise approximately 30% of WCB trajectories (Tab.2). The temporal variations of PV for NPVA GS trajectories, as shown in Fig.4e, display a typical WCB-like behavior. An initial increase in PV from -72 to -48 h followed by a decrease, suggests the release of latent heat due to condensation in WCB-like ascent (Madonna et al., 2014). Indeed the average potential temperature increases from 294 K to 315 K in this time window along with a marked moisture reduction (Fig.4f). Thus the formation of stratiform and convective clouds, as well as precipitation, leads to the release of latent heat, resulting in diabatic heating of rising air masses. The influence of diabatic heating on blocks within the North Atlantic-European region has been underscored by recent research (e.g. Steinfeld and Pfahl, 2019; Steinfeld et al., 2020; Pfahl et al., 2015). Within a 38-year global study, Steinfeld and Pfahl (2019) identified that between 30-45% of trajectories initiated in upper-level blocks underwent diabatic heating. This contrasts slightly with the 51.8% reported by Yamamoto et al. (2021), who suggest that variations in blocking definitions and trajectory approaches could account for the difference. For a quantitative comparison with these studies, we detect diabatic heating in trajectories based on the criterion set by Pfahl et al. (2015), which specifies a change in potential temperature ($\Delta\theta$) of at least 2 K over a 3-day period from the onset of backward trajectories. Our findings indicate that approximately 48% of all trajectories started from the NPVA objects (NPVA base trajectories, see DH Tab.2) underwent diabatic heating in the 3 days leading up to their arrival in the blocking region. This observation aligns with the aforementioned data from previous climatological investigations (Steinfeld and Pfahl, 2019). As anticipated, a larger proportion of ascending trajectories, 63%, undergo diabatic heating compared to just 38% of non-ascending trajectories. This contrast is further amplified when distinguishing between GS and nonGS trajectories within the ascending category, with rates of 98% and 54.7%, respectively. The dominance of diabatic heating in the air masses that interacted with the Gulf Stream is further mirrored by an increase in potential temperature visible in Fig.4b, where NPVA GS trajectories demonstrate on average 21 K rise, which is 7 K more than that in nonGS trajectories

(Tab.2). Building on the insights of Steinfeld and Pfahl (2019); Pfahl et al. (2015), such pronounced diabatic heating, often termed 'latent heating bursts', suggests an interplay between the block and preceding cyclones.

Strong heating occurs also at the surface, as indicated by negative values in the sensible and latent heat fluxes (Fig.4c,d). This heating correlates with the prevalent CAO events across the western and central North Atlantic, as shown in Fig.2. Supporting this, a considerable portion (82%) of NPVA GS trajectories are identified as CAO (Tab.2, see Section 2.1.4), in agreement with the findings presented in Section 3.1. The development of multiple cyclones in the western North Atlantic created conditions favorable for the advection of cold air of continental origin over warmer waters, particularly south of the Gulf Stream. This resulted in enhanced heat and moisture exchanges between the ocean and atmosphere, even leading to the emergence of negative potential vorticity values, signaling an unstable environment (see Appendix A).

Importantly, some CAO events coincided with 'dry intrusions' (DIs), defined by Raveh-Rubin (2017) as the descent of 400 hPa within 48 h. DIs are the descending counterpart to WCBs and typically occur in the cold sector of extratropical cyclones (Raveh-Rubin, 2017). When DIs reach the lower troposphere they affect the atmospheric boundary layer through enhanced surface fluxes, heightened wind speeds, and the elevation of the planetary boundary layer (cf. Ilotoviz et al., 2021). Thus it is worthwhile investigating if NPVA trajectories also feature characteristics of DIs. We find 11.4% of the NPVA GS trajectories featuring DI characteristics, Tab.2). DIs occurred particularly over the southern part of the Gulf Stream, northeast of Florida (not shown). The extreme nature of dry intrusions and their role in potentially triggering intense CAO events prompted us to analyze trajectories that sequentially experience DI, CAO, and diabatic heating (DH). Notably, a majority of DI trajectories follow this sequence ($\sim$80%, cf. Tab.2). Thus, in our case study a DI in the vicinity of the GS has a very high likelihood of later ascent in a WCB-like air stream into the upper troposphere and contribute to blocking. While these trajectories represent a minor portion of all those originating from NPVAs ($\sim$2%), we find this dynamical relevance of DI air streams interacting with the Gulf Stream noteworthy and of potential relevance for subsequent research studies.

Our findings emphasize that while only 28% of all ascending trajectories originate from the block and interact with the Gulf Stream in the lower troposphere, these trajectories display unique features, suggesting pronounced block-cyclone interactions. In addition, while it is widely established that diabatic heating in regions of intense surface heat fluxes influences the large-scale atmospheric circulation (e.g., Pfahl et al., 2015; Yamamoto et al., 2021; Tilinina et al., 2018), the understanding of the mechanistic link between processes that take place within CAOs in the wake of extratropical cyclones and upper-level ridge formation is still missing (Czaja et al., 2019). Our results show that the intense, CAO-induced air-sea interactions in the western North Atlantic and an episode of European Blocking might be inherently linked. Furthermore, the connection between the surface fluxes and coherent air streams hints at a dynamical linkage of the Gulf Stream front to the large-scale atmospheric circulation. In the following section, we aim to further detail this mechanistic link.

3.3 Moisture sources for NPVA GS trajectories

The rapid, cross-isentropic ascent of air parcels into the upper-level NPVA is driven by the latent heat release during cloud formation and precipitation (Joos and Wernli, 2012). For clouds and precipitation to form, a sufficient moisture supply is needed (Eckhardt et al., 2004; Pfahl et al., 2014). Employing the method from (Sodemann et al., 2008), we examined the

moisture sources for the ascent of both NPVA GS and NPVA nonGS trajectories (Tab.1). However, given our paper's primary focus, we primarily concentrate on trajectories that interacted with the Gulf Stream.

First, we will focus on the timing and spatial distribution of moisture uptakes of the trajectories. NPVA GS trajectories, on average, accumulate moisture around 3.5 days before their ascent (Tab.3). Roughly 78% of this moisture is gathered within the seven days leading up to the ascent, with the most significant portion (about 60%) acquired in the first five days. In comparison, NPVA nonGS trajectories start collecting moisture about 3.8 days prior to ascent (Tab.3), with 67% of uptakes taking place within the initial week and 48% within the first five days backward. Interestingly, over a span of 10 days, only 44% of NPVA nonGS trajectories occur over the ocean, in contrast to 78% for NPVA GS trajectories (Tab.3).

Furthermore, from the start of their ascent, NPVA GS trajectories reach the upper-level NPVA in an average of 2.6 days (Tab.3). This is notably quicker than the 6.65 days taken by NPVA nonGS trajectories, implying that the ascent regions for these two trajectories might be distinct.

Figure 5c illustrates the spatial distribution of moisture uptakes for all NPVA GS trajectories. There are two prominent areas of moisture uptake: one close to the Gulf Stream and another over the central North Atlantic. Interestingly, these regions seem to align with the locations of CAOs observed during our study period (Fig.5a). This may suggest that CAOs, and resulting upward latent heat fluxes (Fig.5b), might play a role in the water cycle of NPVA GS trajectories. Examining the specifics of these uptake regions further underscores the significance of certain geographic locations in the moisture collection process. Our moisture source identification methodology indicates that the majority of the moisture originates from regions relatively close to the block (Fig.5e). In particular, 80-90% of the uptakes come directly from the Gulf Stream area, supplemented by uptakes from the eastern Gulf of Mexico. Meanwhile, the central North Atlantic contributes approximately 20% to the total moisture content before ascent.

Conversely, for NPVA nonGS trajectories, moisture is mainly sourced from the regions characterized by weak or absent CAOs and notably diminished surface fluxes (Fig.5a,b). Predominant moisture contributions stem from the Gulf of Mexico's subtropical regions and the Caribbean Sea (Fig.5f). A distinct observation for the NPVA nonGS trajectories is that their moisture uptakes within the Gulf of Mexico are positioned further to the west, compared to those of NPVA GS trajectories (Fig.5e-f).

The primary uptake regions for NPVA GS trajectories not only align with the Gulf Stream SST front but also correspond to areas of intense CAOs (Fig.5a), which seem to play a significant role in the evolution of NPVA GS trajectories. On average, 62% of all moisture uptakes happen during CAO events over the ocean, when the cold, continental air is advected over warmer water surface (green line in Fig. 6b). Some of the moisture uptakes, especially between 19 and 23 February, align with intense SLHF events (Fig.6a). On the other hand, the NPVA nonGS trajectories tell slightly a different story: only 43% experience a CAO during moisture uptake, and the surface evaporation events observed during the same time frame in February were weaker for these trajectories (Fig.6a).

These intense SLHF events are likely tied to pronounced CAOs, potentially triggered by cyclones L1 and L2 (Fig.3). High surface heat fluxes, as pointed out by Tilinina et al. (2018), indicate that the cyclones responsible for these pronounced fluxes usually have greater depth and undergo quicker intensification. Our results support this perspective, as the highest fluxes experienced by NPVA GS air parcels coincide with the period when cyclones L1 and L2 are present in the North Atlantic

(Fig.6a). As depicted in Figure 2d and 2f, both cyclones triggered significant CAO events, which affected many of the NPVA GS air parcels present at the time in the lower troposphere. When focusing specifically on these trajectories, we observe that the average uptakes occurring in CAOs are consistently more intense than those outside CAOs, particularly between 19 to 22 February (Fig.6c). This observation is consistent with insights from other studies (e.g. Papritz and Grams, 2018; Aemisegger and Papritz, 2018; Hawcroft et al., 2012), which highlight the pivotal role of CAOs in moisture-related dynamics. However, it remains poorly understood how air parcels moistened in the region behind a passing cyclone's cold front end up in the upper-level NPVA. One possible explanation is the existence of the so-called 'hand-over' mechanism described in detail by Papritz et al. (2021). They found that moisture precipitating in deep North Atlantic cyclones originates in the cold sector of a preceding cyclone and is fed into the ascent regions of the subsequent cyclone via the feeder air stream (Dacre et al., 2015).

In order to explore the 'hand-over' mechanism in our case study we now use the surface latent heat flux (SLHF) from ERA5 as a proxy for surface evaporation and relate it to the NPVA trajectories. Following the methods of Yamamoto et al. (2021) and Tilinina et al. (2018), we identified regions of maximum SLHF beneath the trajectories to locate the areas of the most intense surface evaporation. We also examined the locations where the trajectory ascent into the upper troposphere begins (Fig.7).

Figure 7a (red contours) illustrates the analysis for 24 February at 21:00 UTC, revealing that when air parcels of NPVA GS trajectories experience the most intense evaporation underneath, they are located below 800 hPa near the Gulf Stream and in areas with the highest CAO index values. The air parcels do not ascend immediately but remain in the atmospheric boundary layer for at least 24 hours, being advected south and southeast with the cold air in the cyclone's cold sector (green contours in Fig.7a). The ascent occurs approximately 54 hours after the maximum SLHF values (blue contours in Fig.7b), suggesting that the ascent might not be caused by the cyclone responsible for strong surface evaporation. Instead, our findings suggest that cyclone L2 (Fig.3a) and subsequent cyclones might have a significant role in lifting the moistened air parcels into the upper troposphere's NPVA. This hypothesis aligns with the insights presented by Papritz et al. (2021). Cyclone L2 traverses and strengthens within the region marked by a strong CAO left in the wake of L1 (Fig.2b and d). This moisture-rich air potentially gets channeled into the ascending flow of the L2 cyclone. Moreover, secondary cyclones following L1 could elevate portions of these air masses into the upper layers (Fig.2c).

To explore whether the process detailed above is dominant in our case study, we conducted the analysis depicted in Figure 7a for all the NPVA GS trajectories (Fig.7c). Analyzed trajectories experience the most intense moistening along the Gulf Stream SST front (red contours). One day later, the moistened air moves south or southeast, together with the air in the cyclone's cold sector (green contours). Trajectories begin their ascent into the upper troposphere (blue contours) on average 3.5 days after reaching maximum SLHF values (Tab.3). This is very much in line with the exemplary trajectory discussed before and in stark contrast to NPVA nonGS trajectories. The latter primarily experience regions of strongest surface evaporation in the subtropics near 20°N, and remain there before making their ascent further north at a later time (Fig.7d). The lingering of NPVA GS trajectories at low levels suggests that the involvement of multiple cyclones might be necessary to create conditions conducive to the moistening of trajectories followed by their ascent.

This notion is further supported by the analysis of the time difference between the time trajectories experienced the strongest moisture uptake and the time when they start to ascend and their pressure drops below 800 hPa (Fig.8). For NPVA GS trajec-

tories, longer delays between strongest moisture uptake and time of ascent are typical (green shading, Fig.8). The probability density function shows a plateau between peaks at 20 hours and 60 hours, Although the density drops thereafter a plateau extending from 70 to 150 hours. The 20-hour peak corresponds to trajectories ascending directly from the Gulf Stream region (blue contours, Fig.7c). The second peak, coupled with the high density of values exceeding 100 hours, implies a significant temporal gap between moisture uptake and the start of ascent for the majority of NPVA GS trajectories. In contrast, NPVA nonGS trajectories show a single peak around 40 h and thus a rather immediate ascent after experiencing the strongest moisture uptake.

The statistics and results presented thus far hint at the potential presence of a 'hand-over' mechanism in our case study. However, to truly identify its presence and understand how signals from the Gulf Stream air-sea interactions are related to the upper troposphere, we delve deeper by computing various metrics for each trajectory's initiation time. These metrics include average trajectory positions, density of strongest moisture uptakes, and the average times of ascent and strongest moisture uptake. Next, we plot these metrics alongside cyclone masks during the times of moisture uptake (represented by green contours) and the start of ascent (represented by red contours). Visual representations of this analysis are provided in figures 9 and 10 and in the Supplementary Materials (for each time step of the case study).

Exemplary we show NPVA GS trajectories initialized on 21 February 2019 at 12:00 UTC and for illustrative purposes distinguish those which initially cross the Gulf Stream on a southeastward track (towards the region south of 30° N and east of 50° W) from those which approach the Gulf Stream from the South. The former subset amounts to about 25% of the NPVA GS dataset for trajectories started on 21 February 2019 at 12:00 UTC. Ten days before their start, these trajectories are positioned over the Gulf Stream region, where they first begin to accumulate moisture (Fig.9a). They subsequently descend further to the central North Atlantic, where they gather the majority of their moisture over a span of several days (purple shading in Fig.9a). On average, this moisture accumulation occurs 192 hours prior to their initialization (green dot, Fig.9a). Following this, their ascent into the upper troposphere starts roughly 123 hours after the moisture uptake (red dot, Fig.9a). It is important to note the presence of cyclones south of Greenland during both the moisture uptake (green contours) and ascent stages (red contours), with each phase associated with distinct cyclones. A substantial number of the moisture uptakes happen in the CAO region (Fig.9b), in the wake of cyclone l0, whereas the ascent primarily occurs in the warm sector of cyclone l1 (Fig.9c).

Also for the remaining majority of the NPVA GS trajectories (75%) started on 21 February 2019 at 12:00 UTC, the Gulf Stream region emerges as the primary moisture source. On average, these trajectories accumulate moisture about 156 hours before their initialization (green dot in Fig.10a). At that time (-156 h) cyclone L0 (green contour) is located south of Greenland, with a CAO event developed in its wake and in the Gulf Stream region (Fig.10b). The ascent of those trajectories takes place $\sim$102 hours later ahead of cyclone L1 (red dot and contours, Fig.10a,c).

While a sequence of cyclones is pivotal for the moistening and ascent of most trajectories in our study, it is the specific trajectories that traverse the central North Atlantic that very clearly exhibit the 'hand-over' mechanism described by Papritz et al. (2021) (Fig.**??**). These represent about 30% of all NPVA GS trajectories, peaking at 65% for some starting times. They most closely align with the 'hand-over' mechanism, as they seem to be fed into the cyclone moving into the central North Atlantic. For the other trajectories (Fig.10), there is less evidence for a 'hand-over' mechanism, thus it is challenging to discern

	NPVA GS trajectories	NPVA nonGS trajectories
Average time of moisture uptake prior to the start of ascent.	-3.5 days (-84 h)	3.8 days (-92 h)
Fraction of moisture supplied within first 5 days backward.	60%	48%
Fraction of moisture uptakes over the ocean.	78%	44%
Average time of ascent start in relation to the time of arrival into the NPVA.	-2.6 days (-63 h)	-6.65 days (-159 h)
Average time in the ABL prior to ascent.	4 days (96 h)	3.8 days (91.2 h)
Average time of continuous SLHF<0 W/m^2 prior to the start of ascent.	2.5 days (60 h)	23 h

Table 3. Summary of general characteristics and moisture sources for NPVA GS and NPVA nonGS trajectories.

whether this mechanism or the sequential appearance of cyclones is more pivotal for their development. Nevertheless, one consistent observation stands out when looking at figures 10a, 9a, and the Supplementary Material: the presence of a cyclone south of Greenland. Intriguingly, while both moisture uptake and ascent events feature a cyclone in this position, distinct cyclones are responsible for each of these processes. This suggests that a series of cyclones plays a pivotal role — initially moistening the NPVA GS trajectories thanks to the passage of one cyclone, and subsequently lifting them into the upper troposphere with a subsequent cyclone. Moisture uptake can occur directly in the wake of a cyclone, during a CAO event initiated by the cyclone's passage, or in the cold sector of secondary cyclones that develop following a strong primary cyclone. This observation is consistent with findings from Papritz et al. (2021) and Dacre et al. (2019). They highlighted the localized origins of moisture sources for North Atlantic cyclones and underscored the significance of consecutive cyclone appearances in shaping the region's moisture cycle.

Based on the above findings, we conclude that during our study period, a succession of cyclones was essential for the evolution of trajectories crossing the Gulf Stream (NPVA GS trajectories). This pathway enabled them to accumulate moisture and subsequently rise into the upper troposphere, thereby influencing the block's dynamics. Our analysis thus sheds light on the mechanisms through which signals from Gulf Stream air-sea interactions reach the upper layers of the atmosphere. This understanding might also clarify why changes in SSTs in the western North Atlantic in model simulations lead to alterations in large-scale dynamics (e.g. Czaja et al., 2019; Athanasiadis et al., 2022; Scaife et al., 2011).

4 Synthesis and Discussion

Our detailed case study of a European Blocking event in February 2019, offers insights into how air-sea interactions over the Gulf Stream may be associated with the dynamics of an upper-level ridge. Although air masses identified as interacting with the Gulf Stream represent roughly 12% of all trajectories originating within the block's region, we show evidence of their disproportional role in maintaining or enhancing the block's persistence. The potential importance of those air masses

for the development of the block can be established based on the results of Steinfeld et al. (2020), who determined that critical features of the block, including extent, strength, and lifetime, are strongly affected by latent heating taking place in the ascending air streams. Our analysis revealed that almost all of the Gulf Stream trajectories (representing $\sim$12% of all NPVA base trajectories and $\sim$28% of all ascending ones, Tab.1,2) experience diabatic heating during the first three days after starting from the blocking region. Additionally, trajectories that interact with the Gulf Stream exhibit a significantly higher proportion of diabatically heated trajectories (98%) than those not traversing the Gulf Stream (54.7%).

Our findings reveal that air often warmed and moistened in the CAO regions induced by one cyclone, ascends into the upper troposphere through the upward air stream of a subsequent cyclone. This observation aligns with studies by Papritz et al. (2021); Dacre et al. (2019) and Sodemann and Stohl (2013), and the process is graphically illustrated in Fig. 11. When cyclone L0 traverses the western North Atlantic, it induces a CAO just behind its cold front (Fig.11a). This event sets the stage for atmospheric boundary layer warming and moistening. The most robust heat fluxes are observed along the Gulf Stream SST front, a consequence of the pronounced air-sea temperature gradient. It is also where the majority of trajectories undergo moisture uptake. Intriguingly, a subset, constituting about 15% in the presented case and referred to as 'recirculating trajectories' (Fig.11a), travels further into the central North Atlantic. As they traverse, these trajectories are exposed to additional moisture from the milder CAOs that form in the aftermath of cyclone L0, as well as from secondary cyclones that emerge in its trail (Fig. 3a). 51 hours later, a new cyclone, labeled L1, emerges at the same spot previously occupied by cyclone L0. This new cyclone has traveled through and gained strength in the regions marked by CAOs - zones of heightened air-sea interactions - originally induced by cyclone L0. Consequently, the pre-moistened and warmed air is channeled into the warm sector of cyclone L1, which provides conditions for its ascent into the upper layers of the troposphere. Overall, in our results, the 'hand-over' mechanism is especially pronounced for trajectories labeled as 'recirculating' ones (Fig.11). Their behavior closely mirrors the feeder air stream concept described by Papritz et al. (2021) and Dacre et al. (2019). While a significant portion of the trajectories show limited evidence for the existence of a 'hand-over' mechanism, our analysis emphasizes a key insight: a minimum of two cyclones is essential for trajectories, which interact with the Gulf Stream, to undergo both moistening and subsequent ascent into the upper troposphere. Additionally, our data highlights a potential preconditioning by a preceding cyclone, creating favorable conditions for the succeeding cyclone. This is evident as cyclones in our study frequently traverse and amplify within CAOs, caused by preceding cyclones (Fig. 2).

The Gulf Stream region serves as an important moisture source for those NPVA trajectories that passed over it in the lower troposphere, in agreement with the results of Yamamoto et al. (2021) and Pfahl et al. (2014). In fact, the Gulf Stream contributes most of the moisture present in the air prior to its ascent. Those findings imply that the moisture sources for extratropical cyclones in the North Atlantic have a regional character and are concentrated in areas where there is a strong ocean-atmosphere temperature contrast. Another area of moistening of the atmospheric boundary layer is found in the central North Atlantic, south of the Gulf Stream's eastward extension. This area is frequently affected by the advection of cold air from the Labrador Sea or the passage of a cyclone, which provides conditions for strong air-sea interactions. In fact, the cyclones recognized as rapidly intensifying propagate into this stretch of the ocean, while several of the secondary cyclones originate

there (Fig.3). The consistent occurrence of cyclones in areas with intense surface evaporation suggests a 'preconditioning' for cyclone development, as described by (Papritz et al., 2021).

It should be noted that the subtropical regions of the Caribbean Seas and eastern North Pacific are significant moisture sources for air streams progressing to the block, with the NPVA nonGS trajectories comprising 72% of the trajectories. However, these air streams predominantly ascend in regions such as the Gulf of Mexico and the Pacific Ocean, which lie outside the main cyclonic activity in the western North Atlantic. Therefore, for the air masses that ascended into the block during the extratropical cyclones of February 2019 in the North Atlantic, these distant moisture sources seem less influential.

A study by Papritz and Grams (2018) suggests that weather regimes modulate the occurrence of CAOs. However, our findings present a more intricate picture where this relationship appears mutual. During our observed period, CAOs predominantly arose due to the advection of cold air in the wake of cold fronts from passing cyclones, particularly in the Gulf Stream region and its extension. Such CAOs not only induce intense surface heat fluxes, which are essential for maintaining baroclinicity (Papritz and Spengler, 2015), but also play pivotal roles in sustaining the storm track (Aemisegger and Papritz, 2018). Furthermore, they promote the formation of rapidly intensifying low-pressure systems, essential for the growth of atmospheric blocks (Colucci, 1985; Colucci and Alberta, 1996). In tandem, these CAOs create conditions favorable for vigorous evaporation events in the western North Atlantic. This abundant moisture aids the swift intensification of cyclones and the genesis of secondary low-pressure systems, contributing to the northward expansion of an upper-level ridge. This, in turn, weakens the zonal flow, paving the way for further CAO development and subsequent intense surface evaporation events (Kautz et al., 2022; Gao et al., 2015). It is also worth noting that these pronounced oceanic evaporation events are instrumental for the emergence of WCBs (Pfahl et al., 2014; Eckhardt et al., 2004), responsible for the emergence of low PV anomalies in the upper troposphere (Pfahl et al., 2015; Steinfeld and Pfahl, 2019; Methven, 2015).

While our study concentrates on a limited set of trajectories in comparison to all initiated from the NPVA objects, such a subset, as suggested earlier, might have implications in the reinforcement or sustenance of the block. Consequently, we hypothesize that the block's termination could be linked to a reduced ocean heat content following the passage of several cyclones. This reduction could diminish air-sea interactions, atmospheric heating, and moistening, which in turn impacts the storm track (as evidenced by the altered pathways of cyclones L3 and L4, Fig.3) and the intensity of the cyclones.

5 Conclusions

To summarize, our study provides a possible explanation for a mechanistic link between air-sea interactions over the Gulf Stream region and the formation of blocks over the North Atlantic and European regions. It also underscores the potential significance of CAOs and the associated strong air-sea interactions in the formation or preservation of a quasi-stationary, upper-level ridge. In light of the growing evidence suggesting that biases in North Atlantic SST representation are linked to model inaccuracies in block prediction (e.g. Athanasiadis et al., 2022; Czaja et al., 2019; Kwon et al., 2020), it is vital to clarify how the processes taking place in the lower troposphere over the western North Atlantic are connected with the dynamics in the upper levels. Additionally, the recurrent influence of SST observed in climatological studies (Michel et al., 2023; Omrani et al.,

2019; Scaife et al., 2011) implies that the mechanisms linking the Gulf Stream, diabatic processes, and large-scale extratropical circulation might hold relevance on a climatological scale. Nevertheless, it is essential to note that a single case study cannot be used to draw any general conclusions. However, considering the fact that singular aspects of our analysis are in agreement with recent publications focusing on moisture transport in the North Atlantic and the formation of blocks (e.g. Papritz et al., 2021; Aemisegger and Papritz, 2018; Hirata et al., 2019; Yamamoto et al., 2021; Steinfeld et al., 2020; Dacre et al., 2019), it provides a basis for further research. Therefore, in a subsequent study, we are going to analyze those relationships using a similar trajectory dataset spanning 40 years of ERA5 data. Using the methods applied in this case study, we will aim to establish whether the air-sea interactions over the Gulf Stream modulate the large-scale dynamics and formation of blocked weather regimes over Europe and to identify the predominant way by which the signal from the lower troposphere is transferred to the upper-level flow.

Appendix A: Negative Potential Vorticity in the lower troposphere

In the course of our study, we consistently observed the presence of negative PV during the inflow stage of trajectories, defined as the phase preceding ascent when trajectories are confined within the atmospheric boundary layer (pressure exceeding 800 hPa). Upon further examination, we found that 82% of NPVA GS trajectories displayed negative PV values at certain intervals prior to their ascent. Given the potential significance of this feature (Methven, 2015), we chose to examine it more closely.

To explore the role of air parcels with negative PV in the formation of upper-level negative PV anomalies (NPVAs) we divided the NPVA GS trajectories into two subsets: those with negative PV (NPVA GS negPV trajectories, 82% of all NPVA GS trajectories) and those with continuous positive PV (NPVA GS posPV trajectories, 18% of NPVA GS trajectories) in the lower troposphere. To investigate the potential influence of negative PV in the lower troposphere on the formation of upper-level NPVA, we examined the inflow and outflow stages of ascent. Specifically, we re-centered the time evolution of the trajectories at the time of maximum heating, which is indicative of the release of latent heat during upward air mass movement. By comparing the two sets of trajectories, we aim to determine whether the presence of negative PV air in the inflow stage of the ascending air stream leads to the formation of low PV air in the upper troposphere. Our results show that the NPVA GS negPV trajectories are located in the lower layers of the troposphere (Fig.A1a) and experience more intensive heating during the ascent (Fig.A1b). Without indicating a cause-and-effect connection, greater fluxes in the inflow stage (Fig.A1c-d) and elevated moisture content during the ascent (Fig.A1f) co-occur with a rise in heating intensity throughout the ascent. Interestingly, despite experiencing negative values of PV in the atmospheric boundary layer and a strong heating rate, the PV of the NPVA GS negPV trajectories is not lower than that of the NPVA GS posPV trajectories in the upper troposphere (Fig.A1e) nor do they reach a higher outflow height (Fig. A1a,b). In fact, the NPVA GS negPV trajectories typically begin at a lower altitude, and as a result, more heating is required for these trajectories to achieve a comparable outflow height to that of the NPVA GS negPV trajectories. Surprisingly, the PV values in the NPVA GS negPV trajectories are even slightly higher when reaching the upper troposphere. Furthermore, we note that air masses with only positive PV values have limited interactions with CAOs. This is evident from the temporal variations of latent and sensible heat fluxes observed in the two trajectory types. In fact, our

565 analysis reveals that 85% of negative PV values are located within CAO regions. This suggests that the processes during CAOs might play a pivotal role in reducing PV in the atmospheric boundary layer.

There are several processes that can result in the destruction of PV in the lower troposphere, including friction, evaporative cooling, sublimation of snow, snow melting, or turbulent fluxes (Crezee et al., 2017; Attinger et al., 2019, 2021). To establish what mechanism leads to PV destruction throughout our case study, we examined vertical cross-sections of cloud liquid water
570 content and potential vorticity over the area of the Gulf Stream. For the purpose of this analysis, we used the ERA5 reanalysis dataset with a higher temporal resolution of 1 hour. Obtained results reveal that the air parcels with negative PV in the lower troposphere are primarily located below liquid water clouds (Fig.A2a), in the cold sectors of the cyclones (Fig.3, Fig.A2c). The cold sector is evident in Figure A2a around 40°N latitude, identifiable by the cloud structure. It can also be discerned in Figure A2b based on the temperature contrast. It should be highlighted that these cross sections represent values averaged between
575 -50° and -60° W. Thus, to accurately assess the locations of air parcels, one should refer to Figures a, b, and c collectively. Clouds in the warm sector of the cyclone extend deep into the atmospheric boundary layer, while the cold sector is dominated by low-level stratiform clouds. Low-level clouds forming during the advection of cold air over the ocean due to the cooling of the surface are classified as stratiform clouds (Painemal et al., 2021). The presence of air parcels with negative PV in those areas suggests that evaporative cooling is the main cause of PV reduction. This was confirmed by Chagnon et al. (2013), who
580 discovered that evaporative cooling in the air descending behind the cold front decreases PV. This idea is further reinforced by the studies of e.g.,Wood (2005), Jensen et al. (2000) and Paluch and Lenschow (1991), who found that evaporative cooling in the sub-cloud layer of stratiform clouds is often triggered by the cooling that results from drizzle evaporation.

In most of the analyzed timesteps (e.g. Fig.A1) the PV in the lower troposphere does not go below -1 PVU. However, for several air parcels, we found values below -2 PVU in the two lowest model layers right behind the cold front. Attinger et al.
585 (2019) and Vannière et al. (2017a) attribute the prevalence of negative PV along the cold front to unstable conditions and high surface fluxes. This applies also to our case, as the high negative PV values are found at low altitudes, in the regions of very intense surface fluxes, mainly during the intensification stage of the extreme cyclones (Fig.3a). Overall, we presume that the combination of strong surface fluxes, heating from the surface, and evaporative cooling from low clouds leads to the development of a highly unstable environment, making the presence of negative PV in our case so widespread.

590 It is worth highlighting that a significant number of air parcels in Figure A2 have negative PV and are positioned ahead of the cold front. Our analysis of consecutive time steps reveals that these parcels are transported to this location due to the advection of cold air that trails the cold front from a preceding cyclone. Given the sequence of cyclones previously described as necessary for the moistening and ascent of trajectories, it is plausible to assume that these air parcels, having interacted with a CAO induced by one cyclone, will subsequently ascend into the upper troposphere with cyclone L1 (Fig.3)

595 To summarize, in contrast to the hypothesis of Methven (2015), which proposes that the average PV of WCB outflow is nearly equal to the PV of its inflow due to an almost negligible net change in models, our study offers a slightly different viewpoint. In the analyzed case study, trajectories with negative PV in the atmospheric boundary layer (ABL) exhibit a somewhat higher PV in the upper troposphere when compared to trajectories with positive PV in the ABL. Therefore, we cannot directly link the

growth of NPVAs to the presence of negative PV in the atmospheric boundary layer. In our case study, negative PV functions more as a marker for an unstable environment and evaporative cooling associated with low-level stratiform clouds.

These findings imply that diabatic PV production and destruction may often not exactly balance during ascent as suggested by Methven (2015). This highlights the potential need for further research on the relationship between diabatic processes and changes in PV in ascending air streams.

Author contributions. MW, CMG, LP, MF planned and designed the case study. MW analyzed the data and wrote the manuscript. CMG, LP, MF gave important guidance during the project and provided feedback on the manuscript.

Competing interests. CMG and LP are members of the editorial board of Weather and Climate Dynamics. The authors have no other competing interests to declare.

Acknowledgements. We gratefully acknowledge the European Centre for Medium-Range Weather Forecasts (ECMWF) for providing the ERA5 reanalysis data set, which was made available through their website http://www.ecmwf.int. We also thank the members of the Large-Scale Dynamics and Predictability group at KIT, as well as Jamie Mathews and Arnaud Czaja from Imperial College London, for their valuable discussions and contributions to this project. Additionally, we extend our thanks to Heini Wernli and Michael Sprenger for providing the Lagranto toolkit and cyclone dataset, which greatly facilitated our analyses. The contributions of MW and MF are funded by the German Research Foundation (DFG; Grant GR 5540/2-1) and the Swiss National Science Foundation (SNSF; Grant 200021E_196978), respectively, as part of the Swiss-German collaborative project "The role of coherent air streams in shaping the Gulf stream's impact on the large-scale extratropical circulation (GULFimpact)." The contribution of CMG is funded by the Helmholtz Association as part of the Young Investigator Group "Sub-seasonal Predictability: Understanding the Role of Diabatic Outflow" (SPREADOUT, grant VH-NG-1243).

References

Aemisegger, F. and Papritz, L.: A Climatology of Strong Large-Scale Ocean Evaporation Events. Part I: Identification, Global Distribution, and Associated Climate Conditions, J. Clim., 31, https://doi.org/10.1175/JCLI-D-17-0591.1, 2018.

Athanasiadis, P., Ogawa, F., Omrani, N.-E., Keenlyside, N., Schiemann, R., Baker, A., Vidale, P., Bellucci, A., Ruggieri, P., Haarsma, R., Roberts, M., Roberts, C., Novak, L., and Gualdi, S.: Mitigating Climate Biases in the Midlatitude North Atlantic by Increasing Model Resolution: SST Gradients and Their Relation to Blocking and the Jet, J. Clim., 35, 3385 – 3406, https://doi.org/10.1175/JCLI-D-21-0515.1, 2022.

Attinger, R., Spreitzer, E., Boettcher, M., Richard, F., Wernli, H., and Joos, H.: Quantifying the role of individual diabatic processes for the formation of PV anomalies in a North Pacific cyclone, Q. J. R. Meteorol. Soc., 145, 2454–2476, https://doi.org/10.1002/qj.3573, 2019.

Attinger, R., Spreitzer, E., Boettcher, M., Wernli, H., and Joos, H.: Systematic assessment of the diabatic processes that modify low-level potential vorticity in extratropical cyclones, Weather Clim. Dynam., 2, 1073–1091, https://doi.org/10.5194/wcd-2-1073-2021, 2021.

Barriopedro, D., Fischer, E., Luterbacher, J., Trigo, R., and García-Herrera, R.: The Hot Summer of 2010: Redrawing the Temperature Record Map of Europe, Science, 332, 220–224, https://doi.org/10.1126/science.1201224, 2011.

Binder, H., Böttcher, M., Joos, H., and Wernli, H.: The role of warm conveyor belts for the intensification of extratropical cyclones in Northern Hemisphere winter, J. Atmos. Sci., 73, 3997–4020, https://doi.org/10.1175/JAS-D-15-0302.1, 2016.

Binder, H., Boettcher, M., Joos, H., Sprenger, M., and Wernli, H.: Vertical cloud structure of warm conveyor belts – a comparison and evaluation of ERA5 reanalysis, CloudSat and CALIPSO data, Weather Clim. Dynam., 1, 577–595, https://doi.org/10.5194/wcd-1-577-2020, 2020.

Boutle, I., Belcher, S., and Plant, R.: Moisture transport in midlatitude cyclones, Q. J. R. Meteorol. Soc., 137, 360–373, https://doi.org/https://doi.org/10.1002/qj.783, 2011.

Büeler, D., Ferranti, L., Magnusson, L., Quinting, J., and Grams, C.: Year-round sub-seasonal forecast skill for Atlantic–European weather regimes, Q. J. R. Meteorol. Soc., 147, 4283–4309, https://doi.org/10.1002/qj.4178, 2021.

Chagnon, J., Gray, S., and Methven, J.: Diabatic processes modifying potential vorticity in a North Atlantic cyclone, Q. J. R. Meteorol. Soc., 139, 1270–1282, https://doi.org/https://doi.org/10.1002/qj.2037, 2013.

Colucci, S.: Explosive Cyclogenesis and Large-Scale Circulation Changes: Implications for Atmospheric Blocking, J. Atmos. Sci., 42, 2701 – 2717, https://doi.org/10.1175/1520-0469(1985)042<2701:ECALSC>2.0.CO;2, 1985.

Colucci, S. and Alberta, T.: Planetary-Scale Climatology of Explosive Cyclogenesis and Blocking, Mon. Weather Rev., 124, 2509 – 2520, https://doi.org/10.1175/1520-0493(1996)124<2509:PSCOEC>2.0.CO;2, 1996.

Crezee, B., Joos, H., and Wernli, H.: The Microphysical Building Blocks of Low-Level Potential Vorticity Anomalies in an Idealized Extratropical Cyclone, J. Atmos. Sci., 74, 1403 – 1416, https://doi.org/10.1175/JAS-D-16-0260.1, 2017.

Czaja, A., Frankignoul, C., Minobe, S., and Vannière, B.: Simulating the Midlatitude Atmospheric Circulation: What Might We Gain From High-Resolution Modeling of Air-Sea Interactions?, Curr. Clim. Change Rep., 5, https://doi.org/10.1007/s40641-019-00148-5, 2019.

Dacre, H., Clark, P., Martinez-Alvarado, O., Stringer, M., and Lavers, D.: How Do Atmospheric Rivers Form?, Bull. Amer. Meteor., 96, 1243 – 1255, https://doi.org/10.1175/BAMS-D-14-00031.1, 2015.

Dacre, H., Martínez-Alvarado, O., and Mbengue, C.: Linking Atmospheric Rivers and Warm Conveyor Belt Airflows, J. Hydrometeor., 20, 1183–1196, https://doi.org/10.1175/JHM-D-18-0175.1, 2019.

Dae, J., Cannon, A., and Yu, B.: Influences of atmospheric blocking on North American summer heatwaves in a changing climate: a comparison of two Canadian Earth system model large ensembles, Clim. Change, 172, https://doi.org/10.1007/s10584-022-03358-3, 2022.

de'Donato, F., Leone, M., Noce, D., Davoli, M., and Michelozzi, P.: The Impact of the February 2012 Cold Spell on Health in Italy Using Surveillance Data, PLOS ONE, 8, 1–9, https://doi.org/10.1371/journal.pone.0061720, 2013.

Demirtaş, M.: The large-scale environment of the European 2012 high-impact cold wave: prolonged upstream and downstream atmospheric blocking, Weather, 72, 297–301, https://doi.org/10.1002/wea.3020, 2017.

Eckhardt, S., Stohl, A., Wernli, H., James, P., Forster, C., and Spichtinger, N.: A 15-Year Climatology of Warm Conveyor Belts, J. Clim., 17, 218 – 237, https://doi.org/10.1175/1520-0442(2004)017<0218:AYCOWC>2.0.CO;2, 2004.

Ferranti, L., Magnusson, L., Vitart, F., and Richardson, D.: How far in advance can we predict changes in large-scale flow leading to severe cold conditions over Europe?, Q. J. R. Meteorol. Soc., 144, 1788–1802, https://doi.org/10.1002/qj.3341, 2018.

Gao, Y., Leung, L., Lu, J., and Masato, G.: Persistent cold air outbreaks over North America in a warming climate, Environ. Res. Lett., 10, https://doi.org/10.1088/1748-9326/10/4/044001, 2015.

Grams, C. and Archambault, H.: The Key Role of Diabatic Outflow in Amplifying the Midlatitude Flow: A Representative Case Study of Weather Systems Surrounding Western North Pacific Extratropical Transition, Mon. Weather. Rev, 144, 3847 – 3869, https://doi.org/10.1175/MWR-D-15-0419.1, 2016.

Grams, C., Wernli, H., Böttcher, M., Čampa, J., Corsmeier, U., Jones, S., Keller, J., Lenz, C.-J., and Wiegand, L.: The key role of diabatic processes in modifying the upper-tropospheric wave guide: a North Atlantic case-study, Q. J. R. Meteorol. Soc., 137, 2174–2193, https://doi.org/10.1002/qj.891, 2011.

Grams, C., Beerli, R., Pfenninger, S., Staffell, I., and Wernli, H.: Balancing Europe's wind-power output through spatial deployment informed by weather regimes, Nat. Clim. Change, 7, https://doi.org/10.1038/nclimate3338, 2017.

Grams, C., Magnusson, L., and Madonna, E.: An Atmospheric Dynamics Perspective on the Amplification and Propagation of Forecast Error in Numerical Weather Prediction Models: A Case Study, Q. J. R. Meteorol. Soc., 144, 2577–2591, https://doi.org/10.1002/qj.3353, 2018.

Grumm, R.: The Central European and Russian Heat Event of July–August 2010, Bull. Amer. Meteor. Soc., 92, 1285 – 1296, https://doi.org/10.1175/2011BAMS3174.1, 2011.

Hauser, S., Teubler, F., Riemer, M., Knippertz, P., and Grams, C.: Towards a diagnostic framework unifying different perspectives on blocking dynamics: insight into a major blocking in the North Atlantic-European region, https://doi.org/10.5194/wcd-2022-44, preprint, 2022.

Hawcroft, M., Shaffrey, L., Hodges, K., and Dacre, H.: How much Northern Hemisphere precipitation is associated with extratropical cyclones?, Geophys. Res. Lett., 39, https://doi.org/10.1029/2012GL053866, 2012.

Hersbach, H., Bell, B., et al.: The ERA5 global reanalysis, Q. J. R. Meteorol. Soc., 146, 1999–2049, https://doi.org/10.1002/qj.3803, 2020.

Hirata, H., Kawamura, R., Nonaka, M., and Tsuboki, K.: Significant Impact of Heat Supply From the Gulf Stream on a "Superbomb" Cyclone in January 2018, Geophys. Res. Lett., 46, 7718–7725, https://doi.org/10.1029/2019GL082995, 2019.

Ilotoviz, E., Ghate, V. P., and Raveh-Rubin, S.: The Impact of Slantwise Descending Dry Intrusions on the Marine Boundary Layer and Air-Sea Interface Over the ARM Eastern North Atlantic Site, Journal of Geophysical Research: Atmospheres, 126, https://doi.org/10.1029/2020JD033879, 2021.

Jensen, J., Lee, S., Krummel, P., Katzfey, J., and Gogoasa, D.: Precipitation in marine cumulus and stratocumulus.: Part I: Thermodynamic and dynamic observations of closed cell circulations and cumulus bands, Atmos. Res., 54, 117–155, https://doi.org/10.1016/S0169-8095(00)00040-5, 2000.

Joos, H. and R.M.Forbes: Impact of different IFS microphysics on a warm conveyor belt and the downstream flow evolution, Q. J. R. Meteorol. Soc., 142, 2727–2739, https://doi.org/10.1002/qj.2863, 2016.

Joos, H. and Wernli, H.: Influence of microphysical processes on the potential vorticity development in a warm conveyor belt: a case-study with the limited-area model COSMO, Q. J. R. Meteorol. Soc., 138, 407–418, https://doi.org/10.1002/qj.934, 2012.

Jullien, N., Vignon, E., Sprenger, M., Aemisegger, F., and Berne, A.: Synoptic conditions and atmospheric moisture pathways associated with virga and precipitation over coastal Adélie Land in Antarctica, The Cryosphere, 14, 1685–1702, https://doi.org/10.5194/tc-14-1685-2020, 2020.

Kautz, L.-A., Martius, O., Pfahl, S., Pinto, J., Ramos, A., Sousa, P., and Woollings, T.: Atmospheric blocking and weather extremes over the Euro-Atlantic sector – a review, Weather Clim. Dynam., 3, 305–336, https://doi.org/10.5194/wcd-3-305-2022, 2022.

Kwon, Y., Alexander, M., Bond, N., Frankignoul, C., Nakamura, H., Qiu, B., and Thompson, L.: Role of the Gulf Stream and Kuroshio–Oyashio Systems in Large-Scale Atmosphere–Ocean Interaction: A Review, J. Clim., 23, 3249 – 3281, https://doi.org/10.1175/2010JCLI3343.1, 2010.

Kwon, Y.-O., Seo, H., Ummenhofer, C., and Joyce, T.: Impact of Multidecadal Variability in Atlantic SST on Winter Atmospheric Blocking, J. Clim., 33, 867 – 892, https://doi.org/10.1175/JCLI-D-19-0324.1, 2020.

Leach, N., Weisheimer, A., Allen, M., and Palmer, T.: Forecast-based attribution of a winter heatwave within the limit of predictability, PNAS, 118, e2112087 118, https://doi.org/10.1073/pnas.2112087118, 2021.

Lupo, A. and Smith, J.: Climatological features of blocking anticyclones in the Northern Hemisphere, Tellus A: Dyn. Meteorol. Oceanogr., 47, 439–456, https://doi.org/10.3402/tellusa.v47i4.11527, 1995.

Madonna, E., Wernli, H., Joos, H., and Martius, O.: Warm Conveyor Belts in the ERA-Interim Dataset (1979–2010). Part I: Climatology and Potential Vorticity Evolution, J. Clim., 27, 3–26, https://doi.org/10.1175/JCLI-D-12-00720.1, 2014.

Matsueda, M. and Palmer, T.: Estimates of flow-dependent predictability of wintertime Euro-Atlantic weather regimes in medium-range forecasts, Q. J. R. Meteorol. Soc., 144, 1012–1027, https://doi.org/10.1002/qj.3265, 2018.

Methven, J.: Potential vorticity in warm conveyor belt outflow, Q. J. R. Meteorol. Soc., 141, 1065–1071, https://doi.org/10.1002/qj.2393, 2015.

Michel, S., Heydt, A., Westen, R., Baatsen, M., and Dijkstra, H.: Increased wintertime European atmospheric blocking frequencies in General Circulation Models with a coupled eddy-permitting ocean, npj Clim. Atmos. Sci., 6, https://doi.org/10.21203/rs.3.rs-1811560/v1, 2023.

Moore, G. and Renfrew, I.: An Assessment of the Surface Turbulent Heat Fluxes from the NCEP–NCAR Reanalysis over the Western Boundary Currents, J. Clim., 15, 2020 – 2037, https://doi.org/10.1175/1520-0442(2002)015<2020:AAOTST>2.0.CO;2, 2002.

Mullen, S.: Transient Eddy Forcing of Blocking Flows, J. Atmos Sci., 44, 3 – 22, https://doi.org/10.1175/1520-0469(1987)044<0003:TEFOBF>2.0.CO;2, 1987.

Nakamura, H. and Wallace, J.: Synoptic Behavior of Baroclinic Eddies during the Blocking Onset, Mon. Weather Rev., 121, 1892 – 1903, https://doi.org/10.1175/1520-0493(1993)121<1892:SBOBED>2.0.CO;2, 1993.

Nakamura, H., Sampe, T., Goto, A., Ohfuchi, W., and Xie, S.: On the importance of midlatitude oceanic frontal zones for the mean state and dominant variability in the tropospheric circulation, Geophys. Res. Lett., 35, https://doi.org/10.1029/2008GL034010, 2008.

Novak, L., Ambaum, M., and Tailleux, R.: The Life Cycle of the North Atlantic Storm Track, J. Atmos. Sci., 72, 821 – 833, https://doi.org/10.1175/JAS-D-14-0082.1, 2015.

Omrani, N.-E., Ogawa, F., Nakamura, H., Keenlyside, N., Lubis, S., and Matthes, K.: Key Role of the Ocean Western Boundary currents in shaping the Northern Hemisphere climate, Scientific Reports, 9, https://doi.org/10.1038/s41598-019-39392-y, 2019.

O'Reilly, C., Minobe, S., Kuwano-Yoshida, A., and Woollings, T.: The Gulf Stream influence on wintertime North Atlantic jet variability, Q. J. R. Meteorol. Soc., 143, 173–183, https://doi.org/h10.1002/qj.2907, 2017.

Painemal, D., Corral, A., Sorooshian, A., M.A.Brunke, et al.: An Overview of Atmospheric Features Over the Western North Atlantic Ocean and North American East Coast—Part 2: Circulation, Boundary Layer, and Clouds, J. Geophys. Res. Atmos., 126, e2020JD033 423, https://doi.org/https://doi.org/10.1029/2020JD033423, 2021.

Paluch, I. R. and Lenschow, D. H.: Stratiform Cloud Formation in the Marine Boundary Layer, J. Atmos. Sci., 48, 2141–2158, https://doi.org/10.1175/1520-0469(1991)0482.0.CO;2, 1991.

Pang, B., Lu, R., and Ren, R.: Influence of Siberian Blocking on Long-Lived Cold Surges over the South China Sea, J. Clim., 33, 6945–6956, https://doi.org/10.1175/JCLI-D-19-0944.1, 2020.

Papritz, L. and Grams, C.: Linking Low-Frequency Large-Scale Circulation Patterns to Cold Air Outbreak Formation in the Northeastern North Atlantic, Geophys. Res. Lett., 45, 2542–2553, https://doi.org/10.1002/2017GL076921, 2018.

Papritz, L. and Spengler, T.: Analysis of the slope of isentropic surfaces and its tendencies over the North Atlantic, Q. J. R. Meteorol. Soc., 141, 3226–3238, https://doi.org/10.1002/qj.2605, 2015.

Papritz, L. and Spengler, T.: A Lagrangian Climatology of Wintertime Cold Air Outbreaks in the Irminger and Nordic Seas and Their Role in Shaping Air–Sea Heat Fluxes, J. Clim., 30, 2717 – 2737, https://doi.org/10.1175/JCLI-D-16-0605.1, 2017.

Papritz, L., Pfahl, S., Sodemann, H., and Wernli, H.: A Climatology of Cold Air Outbreaks and Their Impact on Air–Sea Heat Fluxes in the High-Latitude South Pacific, J. Clim., 28, 342 – 364, https://doi.org/10.1175/JCLI-D-14-00482.1, 2015.

Papritz, L., Aemisegger, F., and Wernli, H.: Sources and Transport Pathways of Precipitating Waters in Cold-Season Deep North Atlantic Cyclones, J. Atmos. Sci., 78, 3349–3368, https://doi.org/10.1175/JAS-D-21-0105.1, 2021.

Pfahl, S., Madonna, E., Boettcher, M., Joos, H., and Wernli, H.: Warm Conveyor Belts in the ERA-Interim Dataset (1979–2010). Part II: Moisture Origin and Relevance for Precipitation, J. Clim., 27, 27–40, https://doi.org/10.1175/JCLI-D-13-00223.1, 2014.

Pfahl, S., Schwierz, C., Croci-Maspoli, M., Grams, C., and Wernli, H.: Importance of latent heat release in ascending air streams for atmospheric blocking, Nat. Geosci., 8, 610–614, https://doi.org/10.1038/ngeo2487, 2015.

Raveh-Rubin, S.: Dry Intrusions: Lagrangian Climatology and Dynamical Impact on the Planetary Boundary Layer, J. Clim., 30, 6661–6682, https://doi.org/10.1175/JCLI-D-16-0782.1, 2017.

Reed, R., Stoelinga, M., and Kuo, Y.-H.: A model-aided study of the origin and evolution of the anomalously high potential vorticity in the inner region of a rapidly deepening marine cyclone, Mon. Weather Rev., 120, 893–913, https://doi.org/10.1175/1520-0493(1992)120<0893:AMASOT>2.0.CO;2, 1992.

Sanders, F. and Gyakum, J.: Synoptic-dynamic climatology of the 'bomb'., https://doi.org/10.1175/1520-0493(1980)108<1589:SDCOT>2.0.CO;2, 1980.

Scaife, A., Copsey, D., Gordon, C., Harris, C., Hinton, T., Keeley, S., O'Neill, A., Roberts, M., and Williams, K.: Improved Atlantic winter blocking in a climate model, Geophys. Res. Lett., 38, https://doi.org/10.1029/2011GL049573, 2011.

Scott, D.: Multivariate density estimation: Theory, practice, and visualization: Second edition, https://doi.org/10.1002/9781118575574, 2015.

Shaw, T., Baldwin, M., Barnes, E., Caballero, R., Garfinkel, C., Hwang, Y.-T., Li, C., O'Gorman, P., et al.: Storm track processes and the opposing influences of climate change, Nat. Geosci., 9, https://doi.org/10.1038/ngeo2783, 2016.

Sheldon, L., Czaja, A., Vannière, B., Morcrette, C., Sohet, B., Casado, M., and Smith, D.: A 'warm path' for Gulf Stream–troposphere interactions, Tellus A: Dyn. Meteorol. Oceanogr., 69, 1299 397, https://doi.org/10.1080/16000870.2017.1299397, 2017.

Sodemann, H. and Stohl, A.: Moisture Origin and Meridional Transport in Atmospheric Rivers and Their Association with Multiple Cyclones, Mon. Weather. Rev., 141, 2850 – 2868, https://doi.org/10.1175/MWR-D-12-00256.1, 2013.

Sodemann, H., Schwierz, C., and Wernli, H.: Interannual variability of Greenland winter precipitation sources: Lagrangian moisture diagnostic and North Atlantic Oscillation influence, J. Geophys. Res., 113, https://doi.org/10.1029/2007JD008503, 2008.

Spensberger, C., Madonna, E., Boettcher, M., Grams, C., Papritz, L., Quinting, J., Röthlisberger, M., Sprenger, M., and Zschenderlein, P.: Dynamics of Concurrent and Sequential Central European and Scandinavian Heatwaves, Q. J. R. Meteorol. Soc., 146, 2998–3013, https://doi.org/10.1002/qj.3822, 2020.

Sprenger, M.: Global climatologies of Eulerian and Lagrangian flow features based on ERA-Interim, Bull. Amer. Meteor. Soc., 98, 1739–1748, 2017.

Sprenger, M. and Wernli, H.: The LAGRANTO Lagrangian analysis tool – version 2.0, Geosci. Model Dev., 8, 2569–2586, https://doi.org/10.5194/gmd-8-2569-2015, 2015.

Steinfeld, D. and Pfahl, S.: The role of latent heating in atmospheric blocking dynamics: a global climatology, Clim. Dyn., 53, https://doi.org/10.1007/s00382-019-04919-6, 2019.

Steinfeld, D., Boettcher, M., Forbes, R., and Pfahl, S.: The sensitivity of atmospheric blocking to upstream latent heating – numerical experiments, Weather Clim. Dynam., 1, 405–426, https://doi.org/10.5194/wcd-1-405-2020, 2020.

Teubler, F. and Riemer, M.: Dynamics of Rossby Wave Packets in a Quantitative Potential Vorticity–Potential Temperature Framework, J. Atmos. Sci., 73, 1063 – 1081, https://doi.org/10.1175/JAS-D-15-0162.1, 2016.

Tilinina, N., Gavrikov, A., and Gulev, S.: Association of the North Atlantic Surface Turbulent Heat Fluxes with Midlatitude Cyclones, Mon. Weather. Rev., 146, 3691 – 3715, https://doi.org/10.1175/MWR-D-17-0291.1, 2018.

Vannière, B., Czaja, A., and Dacre, H.: Contribution of the cold sector of extratropical cyclones to mean state features over the Gulf Stream in winter, Q. J. R. Meteorol. Soc., 143, 1990–2000, https://doi.org/10.1002/qj.3058, 2017a.

Vannière, B., Czaja, A., Dacre, H., and Woollings, T.: A "Cold Path" for the Gulf Stream–Troposphere Connection, J. Clim., 30, 1363–1379, https://doi.org/10.1175/JCLI-D-15-0749.1, 2017b.

Čampa, J. and Wernli, H.: A PV perspective on the vertical structure of mature midlatitude cyclones in the northern hemisphere, J. Atmos. Sci., 69, 725–740, https://doi.org/10.1175/JAS-D-11-050.1, 2012.

Wazneh, H., Gachon, P., deVernal, A., Laprise, R., and Tremblay, B.: Atmospheric blocking events in the North Atlantic: trends and links to climate anomalies and teleconnections, Clim. Dyn., 56, https://doi.org/10.1007/s00382-020-05583-x, 2021.

Wernli, H. and Davies, H.: A Lagrangian-based analysis of extratropical cyclones, I, The method and some applications., Q. J. R. Meteorol. Soc., 123, 467–489, https://doi.org/10.1002/qj.49712353811, 1997.

Wernli, H. and Schwierz, C.: Surface cyclones in the ERA-40 dataset (1958–2001). Part I: Novel identification method and global climatology, J. Atmos. Sci., 63, 2486–2507, 2006.

Wood, R.: Drizzle in Stratiform Boundary Layer Clouds. Part I: Vertical and Horizontal Structure, J. Atmos. Sci., 62, 3011–3033, https://doi.org/10.1175/JAS3529.1, 2005.

Xin, F., Peng, D., Liu, R., and Liu, S.-C.: Moisture sources for the weather pattern classified extreme precipitation in the first rainy season over South China, Int. J. Climatol., 42, 6027–6041, https://doi.org/10.1002/joc.7576, 2022.

Yamamoto, A., Nonaka, M., Martineau, P., Yamazaki, A., Kwon, Y.-O., Nakamura, H., and Taguchi, B.: Oceanic moisture sources contributing to wintertime Euro-Atlantic blocking, WCD, 2, 819–840, https://doi.org/10.5194/wcd-2-819-2021, 2021.

Yamazaki, A. and Itoh, H.: Selective absorption mechanism for the maintenance of blocking, Geophys. Res. Lett., 36, https://doi.org/10.1029/2008GL036770, 2009.

Young, M. and Galvin, J.: The record-breaking warm spell of February 2019 in Britain, the Channel Islands, France and the Netherlands, Weather, 75, 36–45, https://doi.org/10.1002/wea.3664, 2020.

Zhuo, W., Yao, Y., Luo, D., Simmonds, I., and Huang, F.: Combined impact of the cold vortex and atmospheric blocking on cold outbreaks over East Asia and the potential for short-range prediction of such occurrences, Environ. Res. Lett., 17, 084 037, https://doi.org/10.1088/1748-9326/ac8362, 2022.

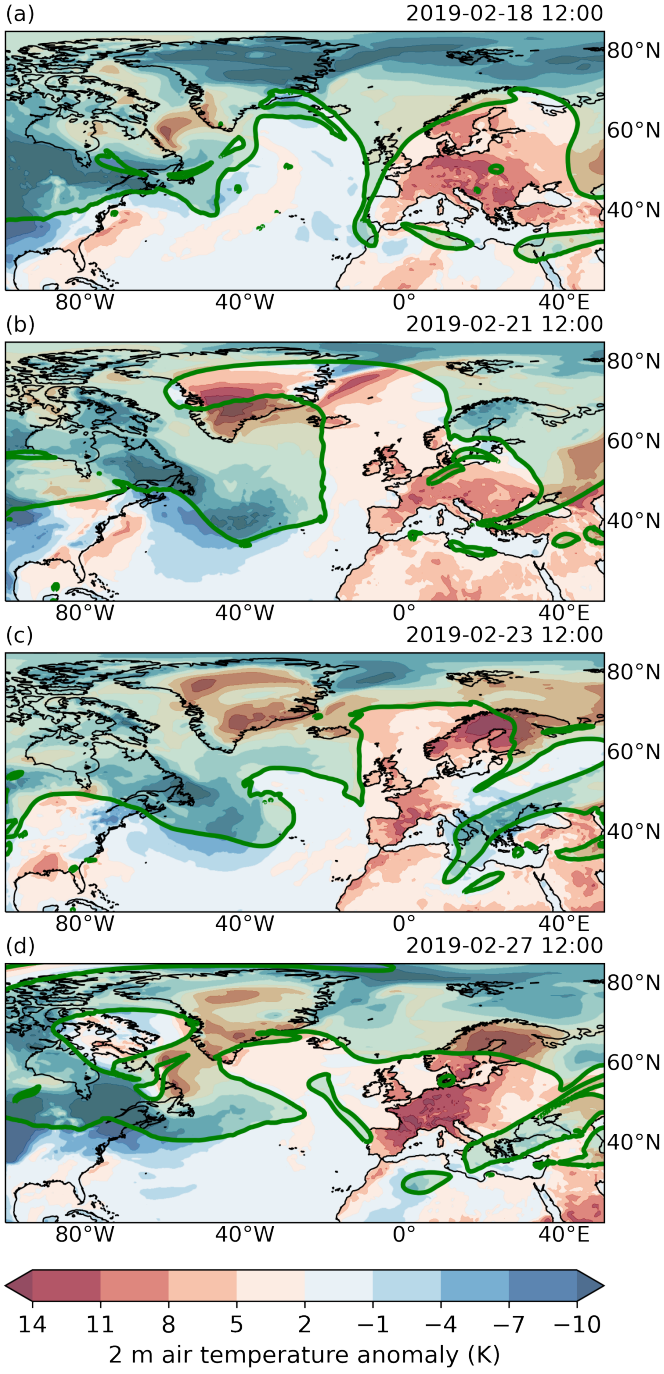

Figure 1. 2 m temperature anomalies (with respect to a 30d running mean, shading) and upper-level 2 PVU contour at 315 K (green line), with PV values higher than 2 PVU shaded in green. Panels are for 12:00 UTC on 18 February 2019 (a), 21 February 2019 (b), 23 February 2019 (c), and 27 February 2019 (d).

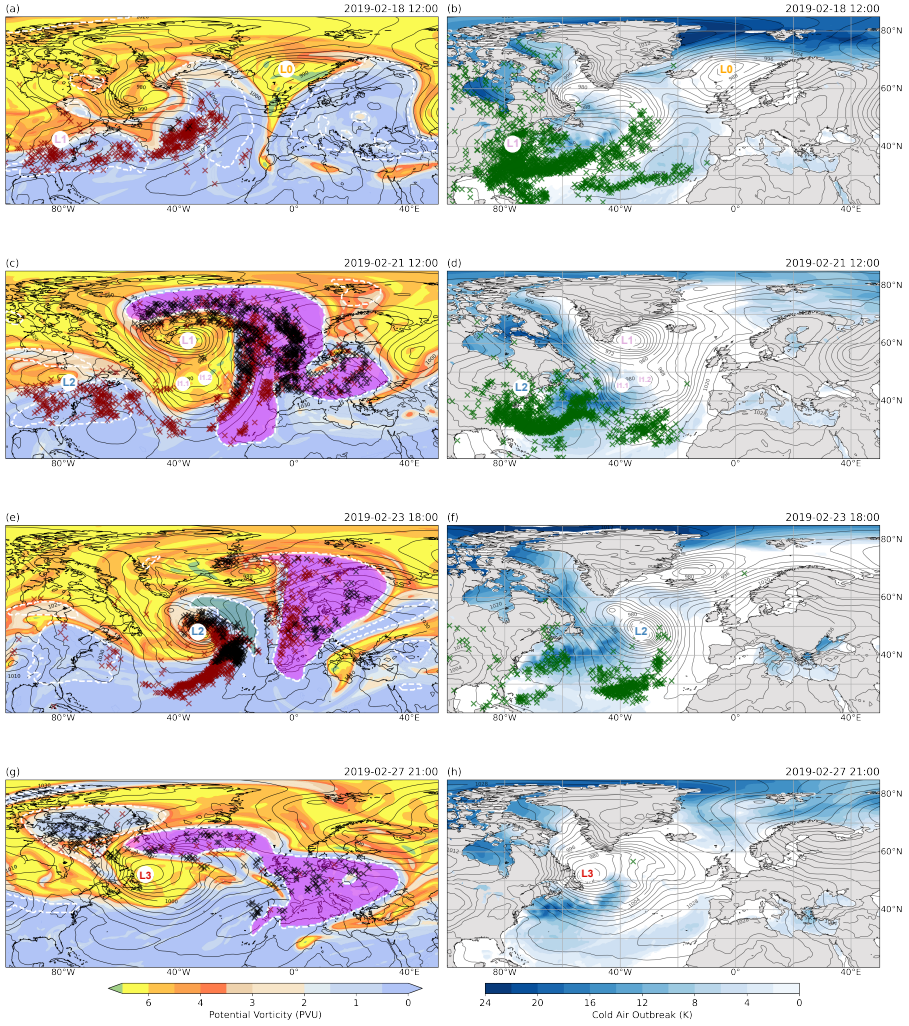

Figure 2. Synoptic evolution of European Blocking episode from February 2019. First column: potential vorticity (shading, PVU) at 315 K and negative potential vorticity anomaly (NPVA) objects (white dashed contours). The major NPVA is shaded in magenta and the minor in light green (Section 2.1.3). Black crosses represent the location of every 30th NPVA GS air parcel at the outflow stage (p >400 hPa)) at the valid time of the panel. Red crosses indicate the locations of every 30th NPVA GS air parcel during the ascent stage (400hPa< p <800 hPa) for the same timestamp. Second column: Cold air outbreak index (shading, K). Green crosses denote the positions of every 30th NPVA GS air parcel at the inflow stage (p >800 hPa) for the corresponding time. Panels are shown for 12:00 UTC 18 February 2019 (a, b), 12:00 UTC 21 February 2019 (c, d), 18:00 UTC 23 February 2019 (e, f), and 21:00 UTC 27 February 2019 (g, h). Black contours in both columns show mean sea level pressure (hPa) and labels L0-L4 refer to the mentioned cyclones with their tracks shown in Fig.3.

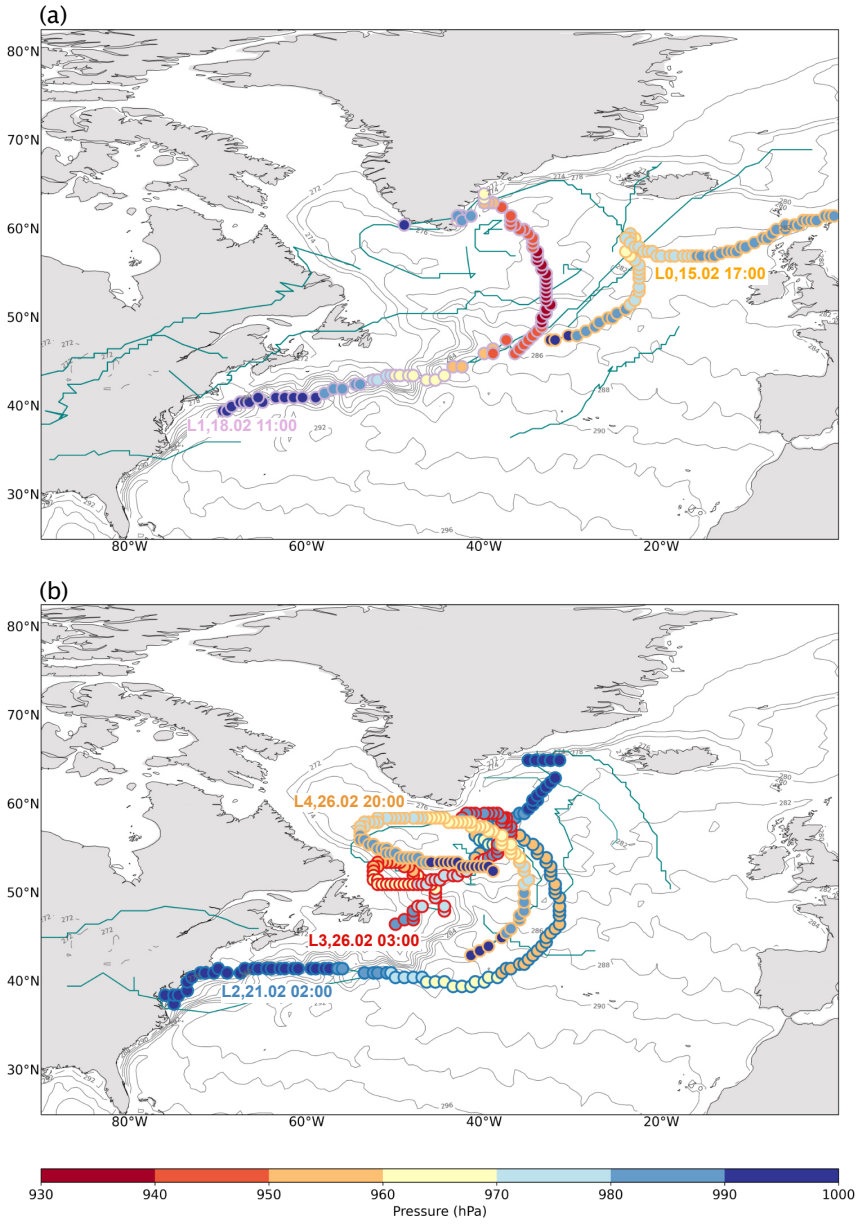

Figure 3. Tracks of cyclones with genesis in the North Atlantic between 15-20 February 2019 (a) and 20-28 February 2019 (b) with contours representing the average sea surface temperature during that period, which serves as an indicator of the Gulf Stream's gradient position. The tracks of rapidly intensifying cyclones (L0-L4, (Sanders and Gyakum, 1980)) are shown by colored circles with the interior color representing minimum sea level pressure. The date near a cyclone's identifier (L0-L4) refers to the genesis time. The tracks of other, non-rapidly intensifying cyclones are shown by thin blue lines.

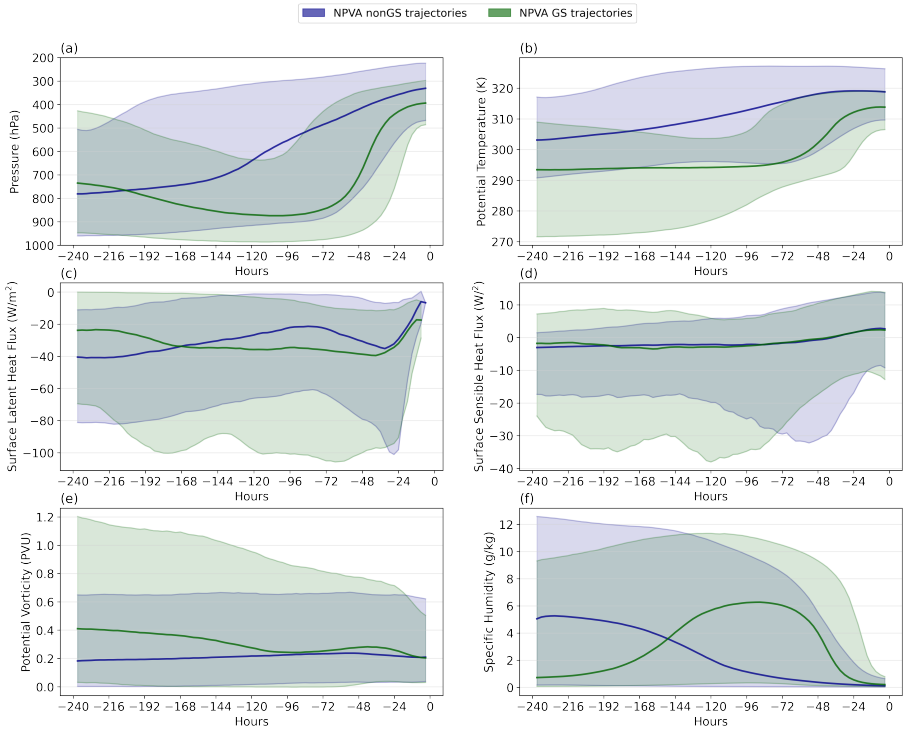

Figure 4. Temporal evolution of (a) pressure, (b) potential temperature, (c) surface latent heat flux, (d) surface sensible heat flux, (e) potential vorticity, (f) specific humidity along NPVA GS (green) and NPVA nonGS (blue) trajectories. Time 0 h refers to the start of the backward trajectory in the NPVA object. The medians are represented as thick lines and the 10th to 90th percentile range is shaded in light green/light blue.

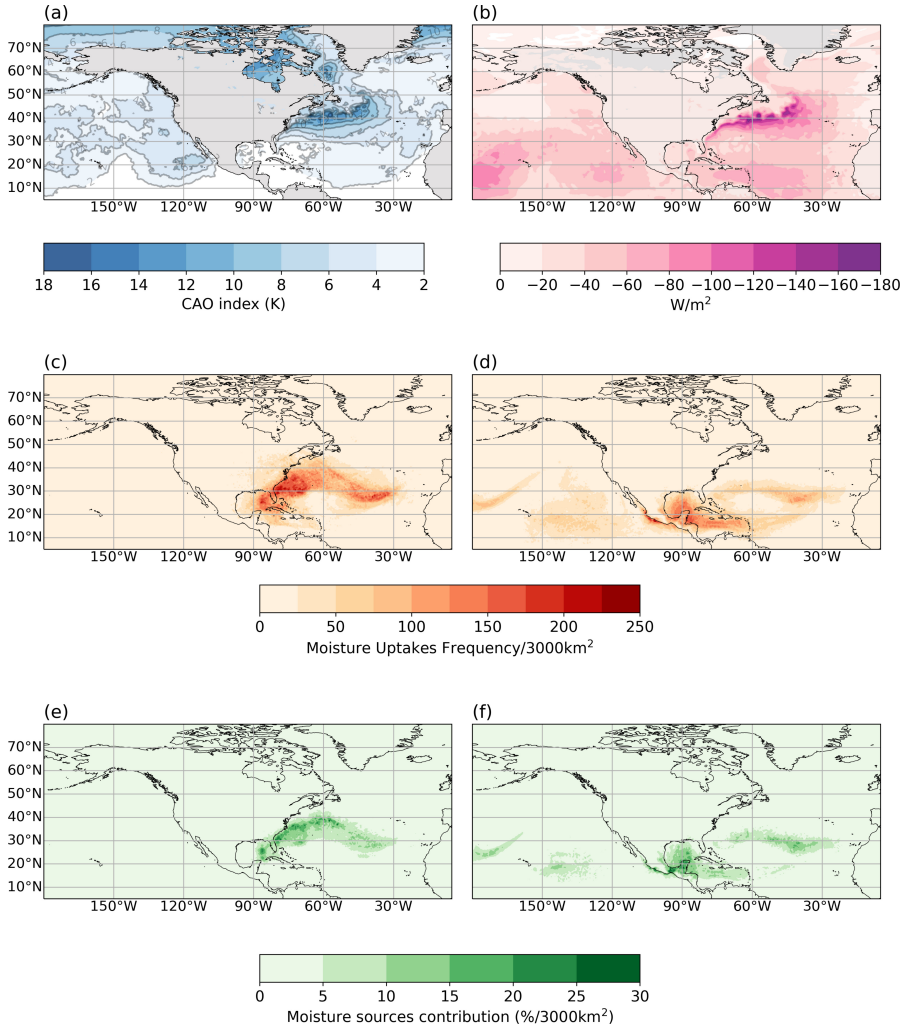

Figure 5. (a) Mean of the 3-hourly CAO index ($\theta_{SST} - \theta_{850}$) during the period from 15 to 28 February 2019 (shading and contours), contours are plotted every 2 K from 2 to 20 K. (b) Same as (a) but for surface latent heat flux (SLHF, shading). Negative SLHF in the ERA5 dataset indicates that SLHF is from the ocean to the atmosphere. (c-f) Analysis of moisture sources for NPVA GS (left column) and NPVA nonGS trajectories (right column; Tab.1). Panels (c, d) show the frequency of moisture uptakes per 3000 km^2 and panels (e, f) the moisture sources contribution to total moisture content present in the trajectory prior to ascent (%/3000 km^2).

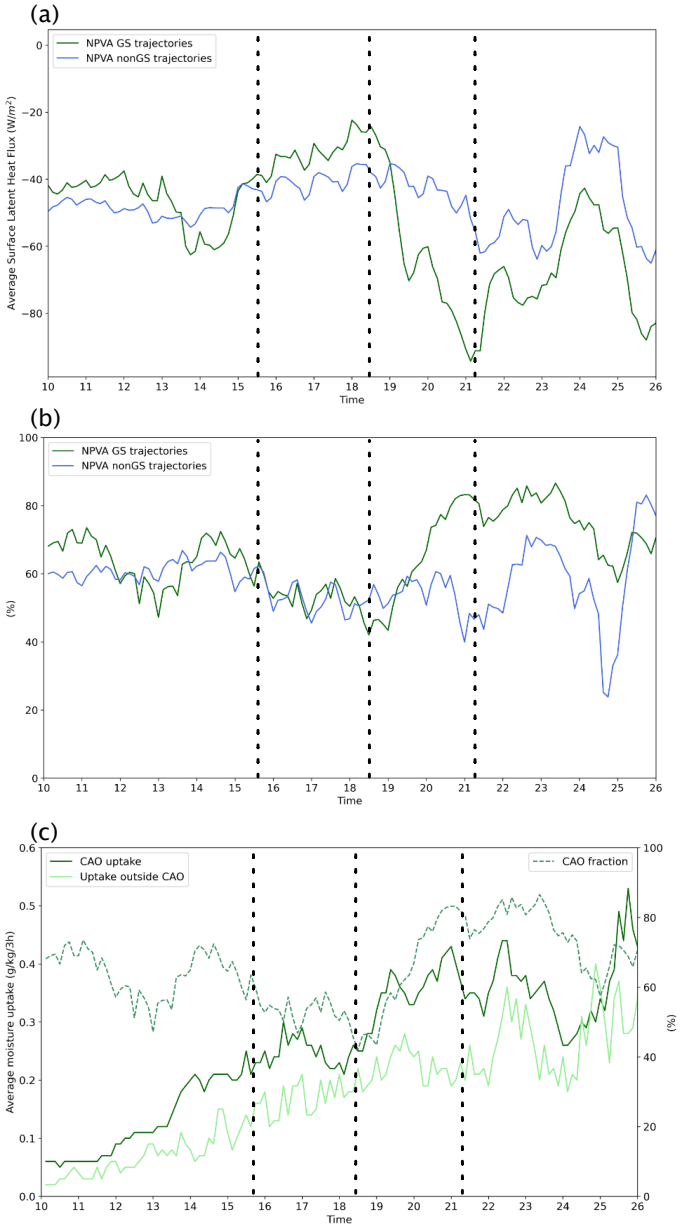

Figure 6. Properties of the air parcels during moisture uptakes. (a) Average surface latent heat flux at the locations of moisture uptakes occurring at the times indicated on the x-axis. The green line represents NPVA GS trajectories, while the blue line denotes NPVA nonGS trajectories. (b) Fraction of moisture uptakes taking place in the CAO regions ($\theta_{SST} - \theta_{850}$), colors correspond to those in (a). (c) Average moisture uptake ($\Delta q = q_t - q_{t+3h}$) for the time specified on the x-axis. The dark green line represents uptakes for NPVA GS trajectories within CAO, while the light green line represents uptakes outside of CAO regions. The green dashed line indicates the fraction of moisture uptakes occurring within CAO regions for NPVA GS trajectories as in (b). Vertical dashed lines refer to cyclogenesis times of cyclones (from left to right): L0, L1, L2 (Fig.3)

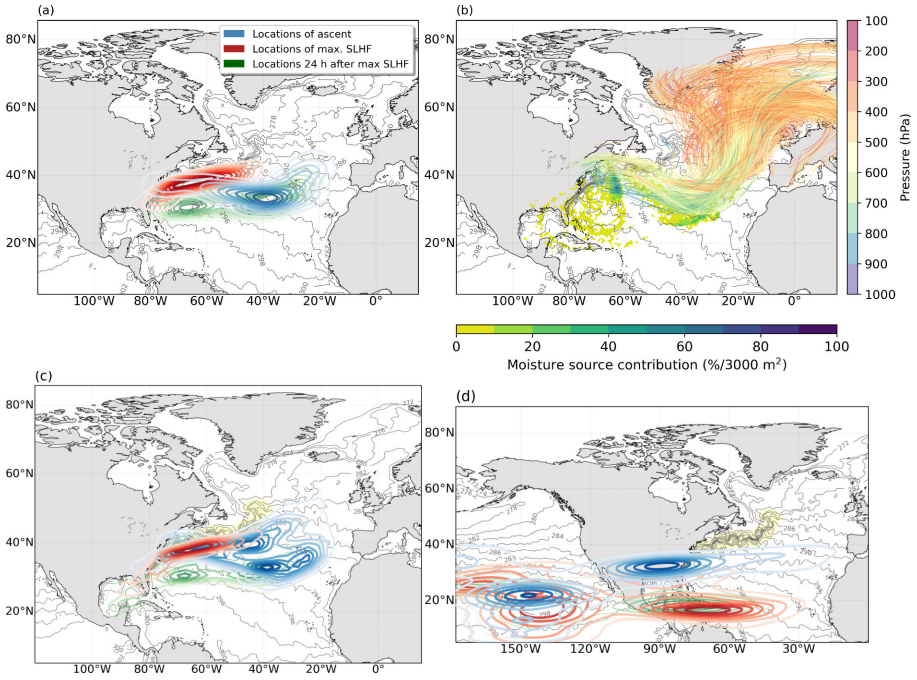

Figure 7. Kernel Density Estimation (KDE; using Scott's rule; Scott (2015)) of air parcel locations at the time of maximum upward surface latent heat flux along trajectories (red contours), 24 h hours later (green contours) and when they start ascending (blue contours) (a) for NPVA GS trajectories started on 24 February at 21:00 UTC, and (c,d) for all trajectories started between 20-28 February 2019 for (c) all the NPVA GS trajectories and for (d) all the NPVA nonGS trajectories. Contours represent 10% steps of the density of air parcels. (b) NPVA GS trajectories started on 24 February at 21:00 UTC colored in pressure height, together with moisture sources' contribution to total moisture present at the time of the start of ascent.

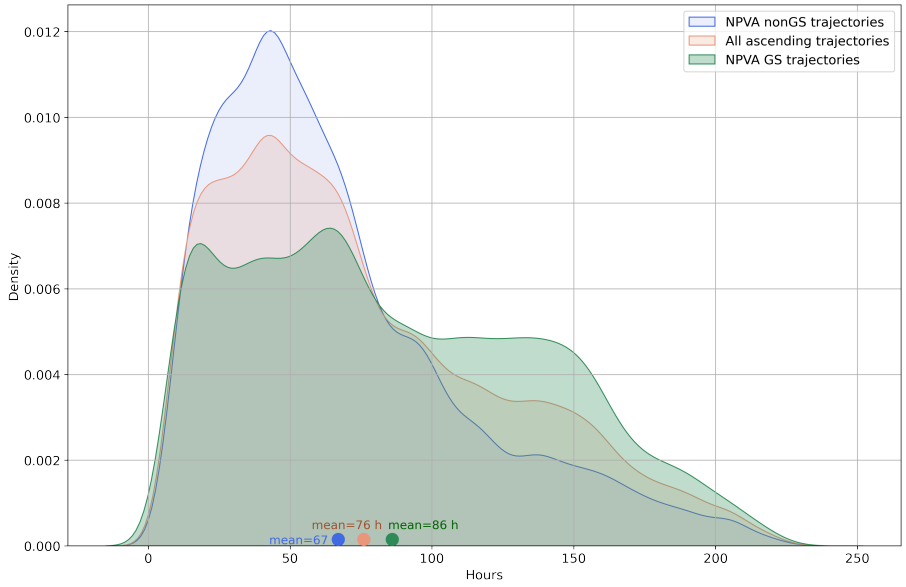

Figure 8. Probability distribution function of the time difference between the strongest moisture uptake and the point at which the pressure decreases to below 800 hPa during the ascent (start of ascent), for NPVA (orange), NPVA GS (green) and NPVA nonGS (blue) trajectories (Tab.1). Dots with labels represent mean values for each set of trajectories.

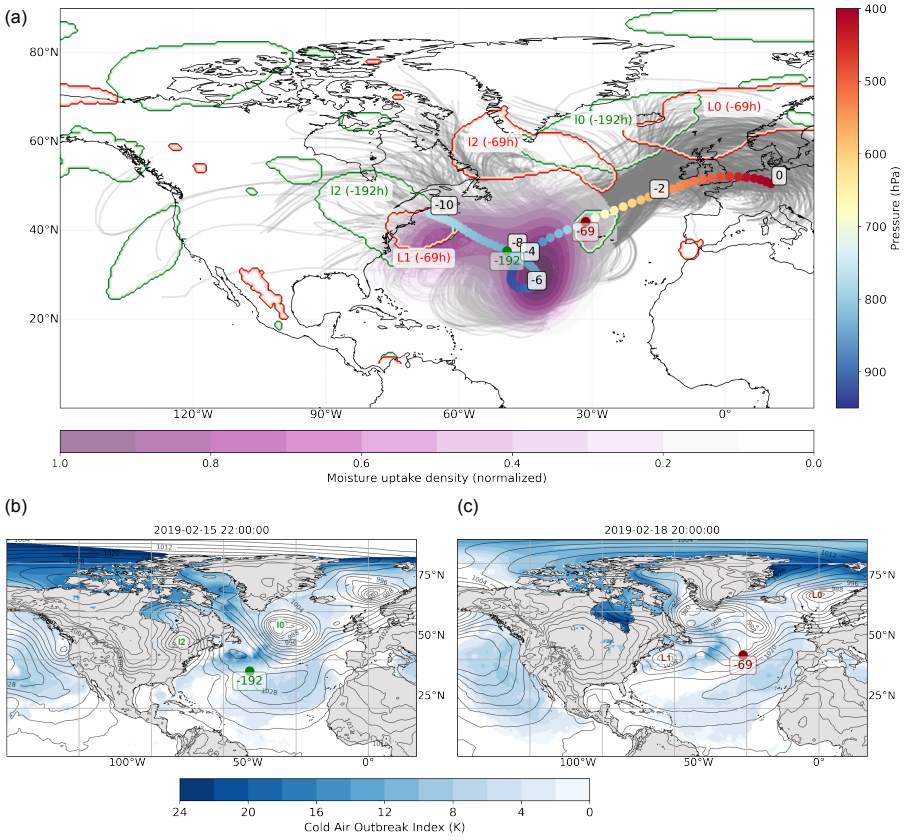

Figure 9. 10-day backward trajectories initialized on 21 February 2019 at 12:00 UTC. (a) Colored dots represent the mean location and pressure (hPa) of trajectories crossing the latitude of 30°N and longitude of 50°W (to southeast), while light grey lines represent individual trajectories used for the calculation of the mean. Black labels mark days prior to arrival in the upper-level NPVA. The green dot (with its corresponding green label) indicates the average moisture uptake time (in hours) for the displayed trajectories, and the green contours outline cyclones present at that moment. The red dot (with its corresponding red label) indicates the average time of start of ascent (in hours) for the displayed trajectories, and the red contours outline cyclones present at that moment. Purple shading represents the normalized (0-1) density of the trajectory positions at the time of most intense moisture uptake. (b) Cold Air Outbreak Index (K) (shading) and mean sea level pressure at the average time of most intense uptake (-192 h), (c) same as (b) but for the average time of start of ascent (-69 h).

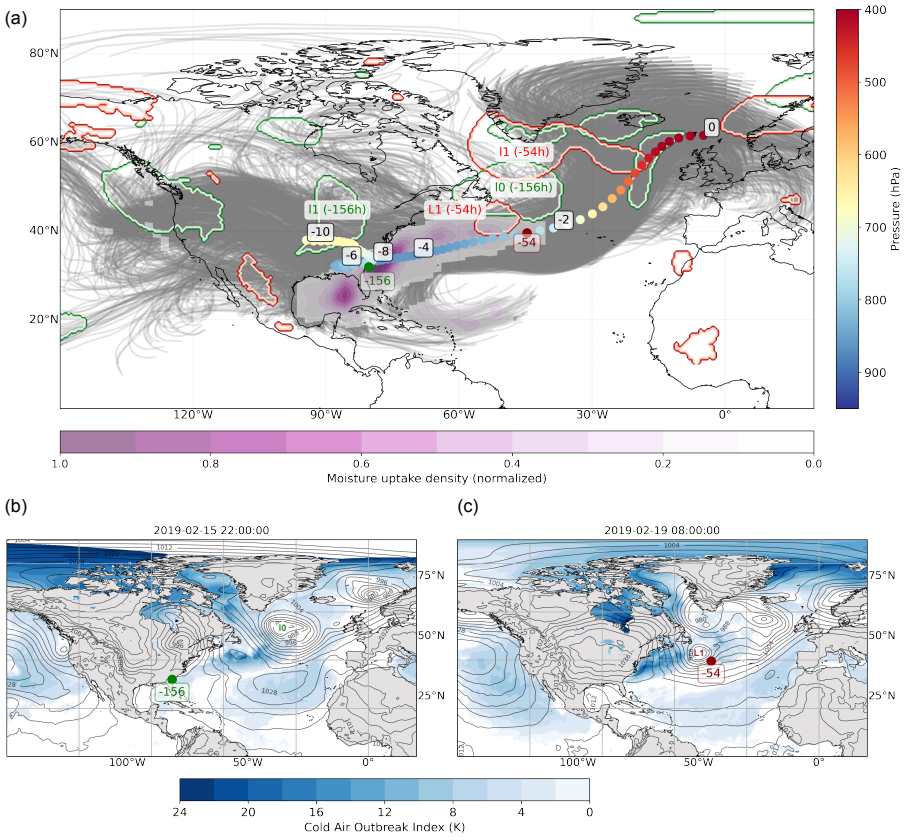

Figure 10. Same as Fig.9 but for trajectories that do not cross over latitude of 30°N and longitude of 50°W.

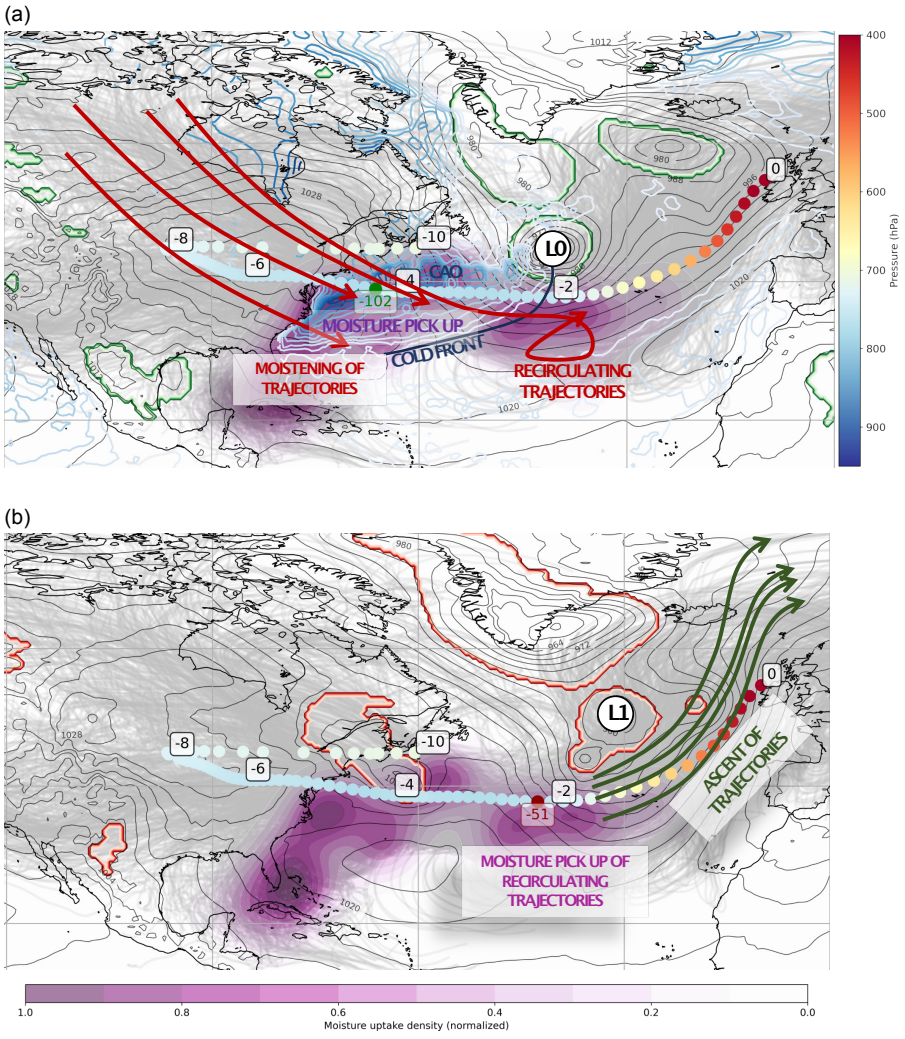

Figure 11. Schematic illustrating the link between cyclones and the pathways of NPVA GS trajectories based on the trajectories initiated from the upper-level NPVA on 24 February at 00:00 UTC. (a) The synoptic situation at the average moisture pick-up time, on 19 February at 18:00 UTC. Black contours depict the mean sea level pressure (hPa), green contours represent cyclone masks, purple shading indicates the normalized density of moisture uptake locations, and blue contours show the cold air outbreak index (K). (b) same as (a) but corresponding to the average start time of trajectory ascent on 21 February at 21:00 UTC, with red contours highlighting cyclone masks.

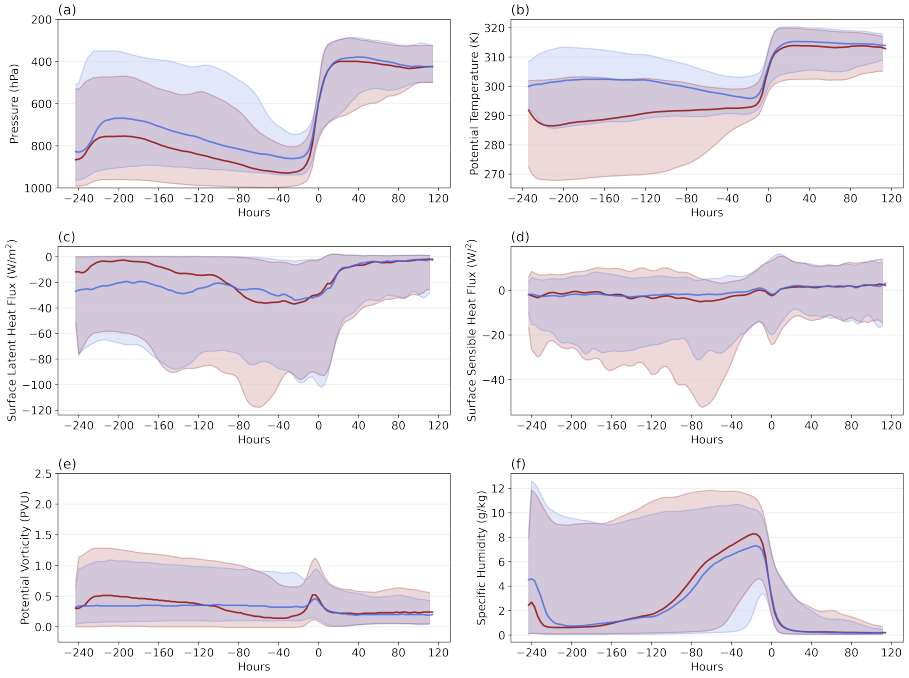

Figure A1. Temporal evolution of: (a) potential vorticity, (b) pressure, (c) surface latent heat flux, (d) surface sensible heat flux, (e) potential temperature, (f) specific humidity along NPVA GS trajectories with negative PV in the atmospheric boundary layer (at least one time step) (red) and with only positive PV (blue). Trajectories are centered on the time step with maximum latent heating (hour 0). The medians are represented as thick red and blue lines and the 90th and 10th percentiles as light red and blue shading.

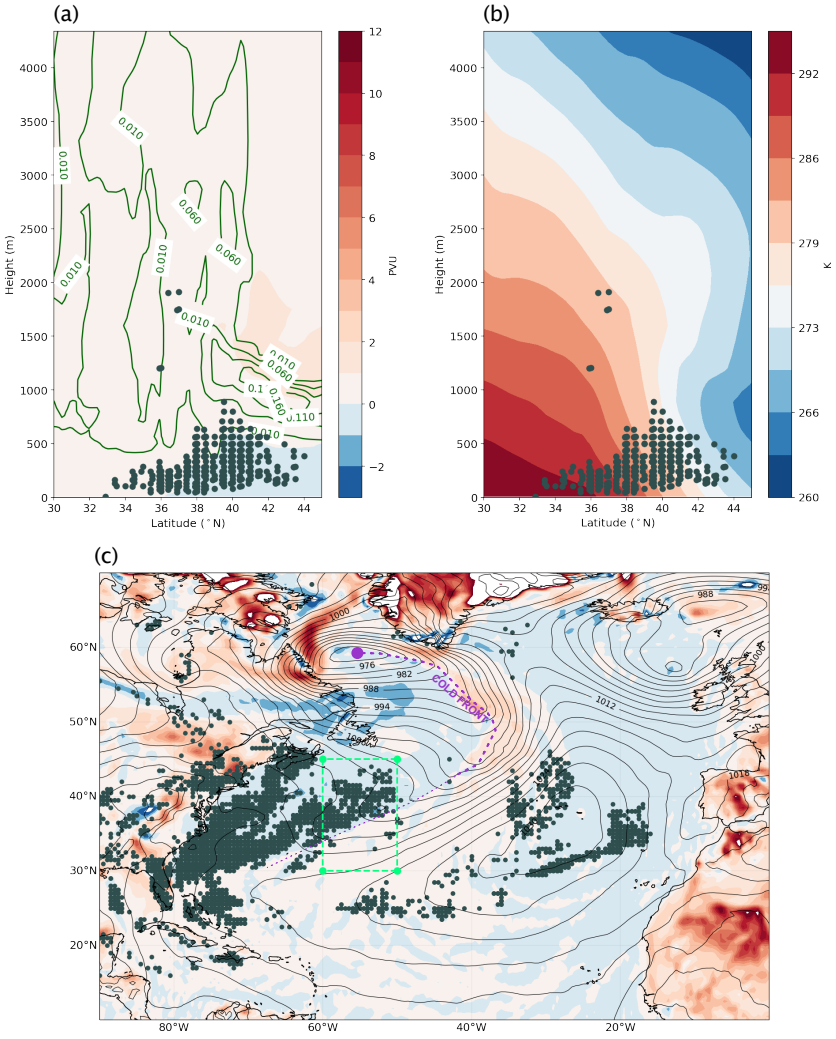

Figure A2. Vertical and horizontal distribution of negative potential vorticity and potential temperature over the area inside the green box in the plot (a) on 18 February at 00:00 UTC. (a) Vertical distribution of potential vorticity (shading) and liquid water content (green contours) averaged over the area between 55° - 60° W and 30° - 45° N, together with the location of all air parcels from the box that have negative PV in the atmospheric boundary layer on 18 February 00:00 UTC. (b) Same as (a) but the contours represent the vertical distribution of potential temperature (shading) averaged over the area between 55° - 60° W and 30° - 45° N,(c) Potential vorticity on the lowest model level and locations of air parcels with negative PV in the atmospheric boundary layer. The plots were created using ERA5 data featuring a 1-hour time resolution.